



## RESEARCH ARTICLE

10.1029/2018JD029703

## Key Points:

- Photochemical box model defines the vertically resolved response of the stratosphere chemical composition to convective perturbation
- Effect of nitric acid removal on column ozone loss is dependent on favorability of initial conditions to heterogeneous chlorine activation
- Nitric acid removal has the most impact on column ozone loss under conditions of mild favorability to chlorine activation

## Supporting Information:

- Supporting Information S1

## Correspondence to:

C. E. Clapp,  
cclapp@fas.harvard.edu

## Citation:

Clapp, C. E., & Anderson, J. G. (2019). Modeling the effect of potential nitric acid removal during convective injection of water vapor over the Central United States on the chemical composition of the lower stratosphere. *Journal of Geophysical Research: Atmospheres*, 124, 9743–9770. <https://doi.org/10.1029/2018JD029703>

Received 22 SEP 2018

Accepted 4 AUG 2019

Accepted article online 7 AUG 2019

Published online 23 AUG 2019

©2019. The Authors.

This is an open access article under the terms of the Creative Commons Attribution-NonCommercial License, which permits use, distribution and reproduction in any medium, provided the original work is properly cited and is not used for commercial purposes.

# Modeling the Effect of Potential Nitric Acid Removal During Convective Injection of Water Vapor Over the Central United States on the Chemical Composition of the Lower Stratosphere

C. E. Clapp<sup>1</sup>  and J. G. Anderson<sup>1,2,3</sup>

<sup>1</sup>Department of Chemistry and Chemical Biology, Harvard University, Cambridge, MA, USA, <sup>2</sup>Harvard John A. Paulson School of Engineering and Applied Sciences, Harvard University, Cambridge, MA, USA, <sup>3</sup>Department of Earth and Planetary Sciences, Harvard University, Cambridge, MA, USA

**Abstract** Tropopause-penetrating convection is a frequent seasonal feature of the Central United States climate. This convection presents the potential for consistent transport of water vapor into the upper troposphere and lower stratosphere (UTLS) through the lofting of ice, which then sublimates. Water vapor enhancements associated with convective ice lofting have been observed in both in situ and satellite measurements. These water vapor enhancements can increase the probability of sulfate aerosol-catalyzed heterogeneous reactions that convert reservoir chlorine (HCl and ClONO<sub>2</sub>) to free radical chlorine (Cl and ClO) that leads to catalytic ozone loss. In addition to water vapor transport, lofted ice may also scavenge nitric acid and further impact the chlorine activation chemistry of the UTLS. We present a photochemical model that resolves the vertical chemical structure of the UTLS to explore the effect of water vapor enhancements and potential additional nitric acid removal. The model is used to define the response of stratospheric column ozone to the range of convective water vapor transported and the temperature variability of the lower stratosphere currently observed over the Central United States in conjunction with potential nitric acid removal and to scenarios of elevated sulfate aerosol surface area density representative of possible future volcanic eruptions or solar radiation management. We find that the effect of HNO<sub>3</sub> removal is dependent on the magnitude of nitric acid removal and has the greatest potential to increase chlorine activation and ozone loss under UTLS conditions that weakly favor the chlorine activation heterogeneous reactions by reducing NO<sub>x</sub> sources.

**Plain Language Summary** Some summertime storms in the Central United States are strong enough to transport water uniquely deep into the atmosphere and up into the normally very dry stratosphere, which houses the ozone layer. Moistening the stratosphere changes its chemical balance. The additional moisture results in the transformation of normally inert halogen compounds, including chlorine and bromine, into chemically highly reactive forms that destroy ozone. This activation of inert halogen compounds and ozone loss is dependent on the amount of water added to the stratosphere and the temperature of the stratosphere. Not every storm that transports water into the stratosphere will result in halogen activation and ozone loss, only those that transport significant amounts of water and/or those that overlap with the coldest parts of the stratosphere. The influence of storms on the chemistry of the stratosphere, however, may not be limited to only water. Nitric acid, which plays a role in slowing the activation of inert halogen compounds, may also be removed. We simulate the chemical effects of a range of potential nitric acid removal in conjunction with moistening of the stratosphere. We find that nitric acid removal has the potential to most exacerbate halogen compound activation and ozone loss when the moistening would normally only have mild effects on the stratosphere. Should nitric acid removal be a common occurrence during these stratosphere-moistening storms, the fraction of storms that can lead to halogen activation and ozone loss is larger than previously thought.

## 1. Introduction

Observations of meteorological conditions in the midlatitudes have indicated the potential for chlorine activation and halogen-catalyzed ozone loss in the lower stratosphere during the summer. Water vapor enhancements resulting from transport by tropopause-penetrating convection, a consistent product of the

unique climate of the summertime Central United States (Anderson et al., 2012; Anderson et al., 2017; Dessler & Sherwood, 2004; Hanisco et al., 2007; Ray et al., 2004; Schwartz et al., 2013; Smith et al., 2017; Sun & Huang, 2015; Toon et al., 2016; E. M. Weinstock et al., 2007), can move the conditions of the lower stratosphere into a state favorable to halogen activation and ozone loss particularly when low temperatures are present. The sensitivity of the lower stratosphere to convective water vapor enhancements is a direct result of the chlorine activation heterogeneous chemistry that is favored by high humidity, low temperatures, and larger sulfate aerosol surface area density (SAD; Anderson et al., 2012; Anderson et al., 2017; Anderson & Clapp, 2018; Carslaw et al., 1997; Drdla & Müller, 2012; Hanson, 1998; Horn et al., 1998; Murphy & Ravishankara, 1994; Portmann et al., 1996; Shi et al., 2001; S. Solomon et al., 1996; S. Solomon, 1999; Tabazadeh et al., 1997). The extent to which potential water vapor enhancements from tropopause-penetrating convective transport may lead to ozone loss in the midlatitude lower stratosphere has been modeled in previous studies (Anderson et al., 2012; Anderson et al., 2017; Anderson & Clapp, 2018).

The impact of an additional, potential convective lower stratospheric perturbation on ozone loss,  $\text{HNO}_3$  scrubbing, however, has not been explored. The current understanding of cross-tropopause water transport through ice lofting could also result in  $\text{HNO}_3$  removal. The potential for stratospheric  $\text{HNO}_3$  removal is a consequence of the primary cross-tropopause water transport mechanism of ice lofting into the lower stratosphere through gravity wave breaking (Hassim & Lane, 2010; Phoenix et al., 2017; Sang et al., 2018; Wang et al., 2011): Ice that sublimates into the lower stratosphere would result in water vapor enhancements, while ice that gravitationally subsides back into the troposphere could scrub stratospheric  $\text{HNO}_3$ . Removal of stratospheric  $\text{HNO}_3$  could potentially increase total chlorine activation resulting from the water vapor enhancements that initiate chlorine activation immediately after convective injection. While observations of water vapor enhancements in the lower stratosphere have been made days after a convective event, the first hours of convective perturbation, including the hypothetical  $\text{HNO}_3$  removal, are not well understood. Additionally, the chemical sensitivity of the lower stratosphere to convective perturbation becomes more important when considering recently proposed solar radiation management (SRM) strategies that would increase the background loading of sulfate aerosol SAD in the lower stratosphere (Dykema et al., 2014; Pitari et al., 2014; Richter et al., 2017; Tilmes et al., 2008; Tilmes et al., 2012). To quantify the extent to which this additional potential effect of  $\text{HNO}_3$  removal by tropopause-penetrating convection may result in ozone loss, we use a photochemical kinetics box model to explore the sensitivity of the chemistry of the lower stratosphere to chemical and physical perturbations associated with convection for sulfate aerosol SAD representative of current and SRM conditions.

Ozone loss in the lower stratosphere is controlled by a network of photochemical reactions first observed by in situ measurements of  $\text{HCl}$ ,  $\text{ClONO}_2$ ,  $\text{ClO}$ ,  $\text{O}_3$ , and so forth in the polar vortices that couple the heterogeneous activation of inorganic chlorine to the gas phase halogen-catalyzed ozone loss cycles (Anderson et al., 2012; Brune et al., 1990; Carslaw et al., 1997; Chipperfield & Pyle, 1998; Drdla & Müller, 2012; McElroy et al., 1986; Portmann et al., 1996; S. Solomon et al., 1986; S. Solomon, 1999; Stimpfle et al., 1999; Wilmouth et al., 2006). These same reactions have also been identified as responsible for chlorine activation in the midlatitudes (Fahey et al., 1993; Hofmann et al., 1994; Kawa et al., 1997; S. Solomon et al., 1998; Wennberg et al., 1994; Wilson et al., 1993) and the tropics (von Hobe et al., 2011). These reactions (1) define the key chemical species, the concentrations of which determine if the lower stratosphere is in a state dominated by halogen-catalyzed ozone loss or not; (2) define the chemical pathway (sulfate aerosol heterogeneous chlorine activation) that transitions the stratosphere from a benign state to a state conducive to ozone loss (as shown in Figure 1); and most importantly (3) define the meteorological conditions that favor chlorine activation on sulfate aerosols (Anderson et al., 2012; Anderson et al., 2017; Carslaw et al., 1997; Drdla & Müller, 2012; Murphy & Murphy & Ravishankara, 1994; Portmann et al., 1996; Shi et al., 2001; S. Solomon, 1999; Tabazadeh et al., 1997). Tropopause penetrating convective transport can affect ozone loss in the lower stratosphere by altering concentrations of some of these key chemical species (in this paper,  $\text{H}_2\text{O}$  and  $\text{HNO}_3$ ).

The key chemical species, which include reservoir inorganic chlorine,  $\text{HCl}$  and  $\text{ClONO}_2$ ; free radical chlorine,  $\text{Cl}$  and  $\text{ClO}$ ; free radical bromine,  $\text{Br}$  and  $\text{BrO}$ ; and the nitrogen species of  $\text{NO}_x$  ( $\text{NO}$ , and  $\text{NO}_2$ ),  $\text{HNO}_3$  and  $\text{N}_2\text{O}_5$ , and their interactions that determine the stratospheric state with respect to halogen-catalyzed ozone loss are shown in Figure 1. The partitioning of inorganic chlorine between its reservoir species (no

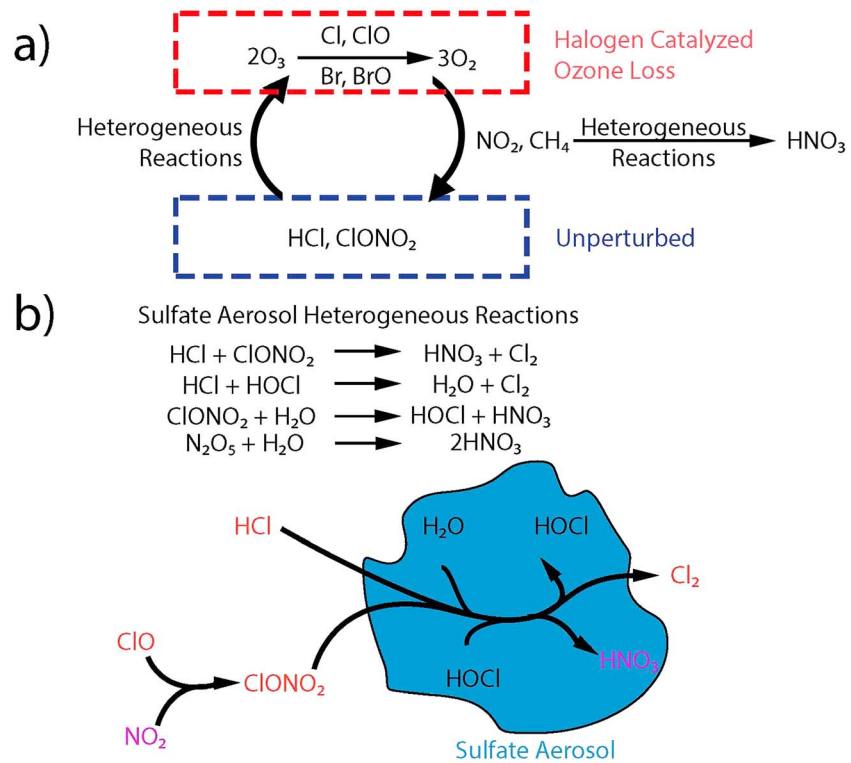
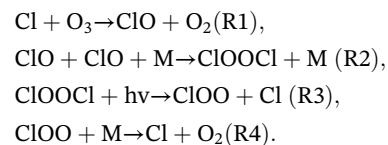
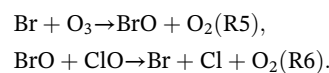


**Figure 1.** (a) The chemistry of the lower stratosphere can be divided into two regimes: an unperturbed regime (blue box) characterized by inorganic chlorine ozone neutral forms of HCl and ClONO<sub>2</sub> and high concentrations of NO<sub>x</sub> and a halogen-catalyzed ozone loss regime (red box) characterized by a significant proportion of chlorine present in the free radical forms of ClO and Cl and low concentrations of NO<sub>x</sub>. The sulfate aerosol-catalyzed heterogeneous reactions move the stratosphere from the unperturbed regime into the halogen-catalyzed ozone loss regime. The reaction of ClO with NO<sub>2</sub> returns the stratosphere to the unperturbed regime. (b) The sulfate-catalyzed heterogeneous reactions have the effect of (1) converting reservoir chlorine to free radical chlorine (in red) and (2) converting NO<sub>2</sub> to aqueous HNO<sub>3</sub> (in purple) that is sequestered in the sulfate aerosol preventing the return of the stratosphere to the unperturbed regime.

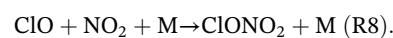
halogen-catalyzed ozone loss) and its free radical form (halogen-catalyzed ozone loss) defines whether the stratosphere is in an unperturbed or halogen-catalyzed ozone loss state. When in its free radical form, inorganic chlorine destroys ozone through a ClO catalytic cycle that involves the ClOOC1 dimer that is only stable at low temperatures (Molina & Molina, 1987):



Free radical bromine participates in an additional catalytic cycle to destroy ozone (McElroy et al., 1986):

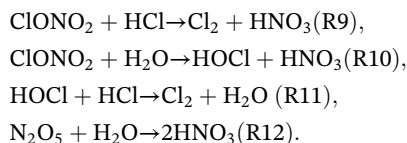


The nitrogen species, while present in the lower stratosphere, through the reaction of NO<sub>2</sub> with ClO to form ClONO<sub>2</sub>, prevent the buildup of free radical chlorine by returning it to the reservoir form:



As a result of these reactions, a state of halogen-catalyzed ozone loss can be characterized by a high ratio of free radical chlorine to inorganic chlorine and low concentrations of  $\text{NO}_x$ . The inverse is true for the unperturbed state.

The following heterogeneous reactions catalyzed by sulfate aerosols transition the stratosphere from an unperturbed state to a state of ozone loss by both converting  $\text{ClONO}_2$  and  $\text{HCl}$  to  $\text{Cl}$  and  $\text{ClO}$  and by depleting  $\text{NO}_x$  (Molina, 1989; Solomon et al., 1986; see Figure 1):



The  $\text{Cl}_2$  produced is photolyzed to form the chlorine radical that reacts with ozone in the Molina mechanism producing  $\text{ClO}$ . The above reactions also deplete  $\text{NO}_2$  by converting  $\text{ClONO}_2$  to aqueous  $\text{HNO}_3$  and  $\text{N}_2\text{O}_5$  to aqueous  $\text{HNO}_3$ . The rates of R9, R10, and R11 are proportional to the uptake probability of the reactants on the catalytic surface, in this case sulfate aerosol, and the reactive SAD. The uptake probability depends on the solubility of the reactants,  $\text{HCl}$ ,  $\text{ClONO}_2$ , and  $\text{HOCl}$  in the sulfate aerosol, which have been shown to be favored by low temperatures and high water vapor concentrations (Hanson, 1998; Horn et al., 1998; Shi et al., 2001).

Although most observations of heterogeneous chlorine activation and the resulting ozone loss come from the polar regions, observations of this mechanisms occurring in the stratosphere at the midlatitudes have been made during the increase in stratospheric sulfate SAD due to the Mt. Pinatubo eruption (Avallone et al., 1993; Fahey et al., 1993; Hofmann et al., 1994; McGee et al., 1994; Solomon et al., 1998; Wennberg et al., 1994; Wilson et al., 1993) and also under standard conditions (Keim et al., 1996; Thornton et al., 2007) near the tropopause.

Tropopause-penetrating convective transport of water directly influences potential ozone loss in the midlatitudes lower stratosphere by increasing the probability of the chlorine activation heterogeneous reactions. Convective overshoots have been shown to moisten the lower stratosphere primarily through the lofting of ice particles in observational (Corti et al., 2008; de Reus et al., 2009; Hanisco et al., 2007; Hegglin et al., 2004; Homeyer, 2014; Homeyer et al., 2017; Iwasaki et al., 2010; Khaykin et al., 2009; Khaykin et al., 2016; Poulida & Dickerson, 1996; Randel et al., 2012; Ray et al., 2004; Sargent et al., 2014; Sayres et al., 2010; Smith et al., 2017; Weinstock et al., 2007) and modeling studies (Dessler et al., 2007; Dessler & Sherwood, 2004; Grosvenor et al., 2007; Jensen et al., 2007; Wang, 2003) in both the tropics and the extratropics. The lower stratosphere is convectively moistened primarily by sublimation of ice that has been lofted into the stratosphere via gravity wave breaking, which is distinct from moistening by convective air mass transport from the troposphere, that is, water vapor transport limited by saturation vapor pressure near the tropopause (Hassim & Lane, 2010; Phoenix et al., 2017; Sang et al., 2018; Wang et al., 2011). The convective lofting of ice into the lower stratosphere by overshoots can even transport ice to higher altitudes beyond the altitude reached by convective ascent (Phoenix et al., 2017; Wang et al., 2011).

As a result of the ice lofting and sublimation transport mechanism, tropopause penetrating convection can lead to stratospheric water vapor enhancements without significant changes to the background chemical composition of the lower stratosphere because small volumes of convectively transported tropospheric air can contain significant quantities of water as ice. Observations of both ozone and carbon monoxide concurrent with water vapor enhancements in the lower stratosphere have shown either no tropospheric signal in the Deep Convective Clouds and Chemistry field campaign (Phoenix et al., 2017) or even possible evidence of downward mixing in the Stratospheric-Climate Links with Emphasis on the Upper Troposphere and Lower Stratosphere field campaign (Frey et al., 2015). Phoenix et al. (2017) conducted a modeling study of cross-tropopause convective transport considering two distinct transport processes: air mass mixing (which could transport tropospheric air in addition to water vapor) and sublimation of convectively lofted ice (which would transport only water). Phoenix et al. (2017) concluded that, although deep convection does rapidly transport air from the troposphere to the stratosphere, most of the stratospheric water vapor enhancements (especially at higher altitudes) are due to the lofting and sublimation of ice with little

tropospheric air mixing resulting in elevated water vapor with little impact on O<sub>3</sub> and CO. In their modeling of deep convection, Frey et al. (2015) find that tropopause penetrating convection both transports boundary layer air upward into the tropical tropopause layer (TTL) and transports ozone-rich stratospheric air downward into the lower stratosphere and the TTL. Frey et al. (2015) also find that tropopause penetrating convection hydrates both the upper TTL and lower stratosphere through ice sublimation resulting in the potential for an overlap of elevated water vapor with elevated ozone in the lower stratosphere.

Modeling studies not informed by observed stratospheric tracers also support ice sublimation rather than air mass transport as the primary mechanism of stratospheric moistening by overshooting convection (Hassim & Lane, 2010; Sang et al., 2018). Sang et al. (2018) specifically find that ice sublimation is the primary contributor to convective stratospheric moistening compared to air mixing, which is a weak contributor. Further, dynamical modeling studies also demonstrate downward mixing from higher altitudes in the stratosphere (Dauhut et al., 2018; Hassim & Lane, 2010).

The dynamic processes involved with convective cross-tropopause transport are not fully understood due to the sparseness of in situ observational constraints. For example, while water transport seems to be controlled by ice lofting with little tropospheric air mixing, observations of aerosol-poor tropospheric air convectively transported into the lower stratosphere indicate that cross-tropopause convection may also result in significant air mass fluxes (Vernier et al., 2011). Similarly, a satellite study of convective overshoots into the lower stratosphere found both that, during convection, ice sublimation likely leads to stratospheric hydration and that either mixing of the overshoot with warmer stratosphere or downward motion adjacent to the updraft results in warmer brightness temperatures than expected (Iwasaki et al., 2012). Regardless of the uncertainty around convective air mass mixing, because water is convectively transported in the solid phase, convective enhancements to water vapor are expected to be far more significant than perturbations to other species in the stratosphere, as has been reported by observations of convective stratospheric perturbations (Frey et al., 2015; Phoenix et al., 2017).

Furthermore, observations of convective overshoots that reach the lower stratosphere over the Central United States during the summer suggest that convective moistening of the stratosphere may be frequent and that these enhancements can remain cohesive in the stratosphere for significant periods of time. Tropopause-penetrating convection at least 1 km above the tropopause occurs over the Central United States during the summer with a frequency of approximately  $0.9 \times 10^4$  events per month, according to a 10-year NEXRAD climatology analysis by Cooney et al. (2018). Observations of water vapor enhancements in coherent plumes have also been made up to between 7 and 12 days after convective injection (Pittman et al., 2007; Ray et al., 2004; Weinstock et al., 2007). Observations of a convectively sourced stratospheric water vapor plume show a minimum spatial extent of 20,000 km<sup>2</sup> between the pressure levels of 70 and 115 hPa and estimate a potentially more realistic area of up to 100,000 km<sup>2</sup> at 115 hPa given the exponential altitude dependence of convective volumes in the lower stratosphere (Smith et al., 2017).

Additionally, deep convection may also affect ozone loss by removing stratospheric HNO<sub>3</sub> from a lower stratospheric air mass thereby removing a source of NO<sub>x</sub>, which has an inhibitory effect on chlorine activation. The uptake of stratospheric HNO<sub>3</sub> onto convectively lofted ice particles that do not sublimate to moisten the lower stratosphere during transit through the stratosphere but rather through selective gravitational subsidence that reenters the troposphere may result in a depletion of HNO<sub>3</sub> in the convectively influenced lower stratospheric air mass. Modeling of tropopause-penetrating overshooting convection has indicated that the larger ice particles convectively lofted into the stratosphere preferentially sediment out of the stratosphere even as the lighter ice particles sublimate (Sang et al., 2018). Therefore, while nitric acid uptake may occur onto convectively lofted ice particles of all sizes, the size selection modeled by Sang et al. (2018), which leads to the larger ice particles sedimenting out of the stratosphere while the smaller ice particles sublimate into the stratosphere, could hypothetically result in the concurrent removal of nitric acid from, as well as moistening of, the lower stratosphere. The uptake of gaseous HNO<sub>3</sub> on ice surfaces has been demonstrated in laboratory studies at atmospherically relevant conditions (Abbatt, 1997; Abbatt, 2003; Aguzzi & Rossi, 2001; Huthwelker et al., 2006; Hynes et al., 2002; Ullerstam & Abbatt, 2005; Zondlo et al., 1997), as well as observed in field studies in the UTLS (Gamblin et al., 2007; Kondo et al., 2003; Krämer et al., 2008; Popp et al., 2004; Popp et al., 2006; Scheuer et al., 2010; Voigt et al., 2006; Voigt et al., 2007). Further, HNO<sub>3</sub> scavenging by

convection through ice uptake has also been demonstrated in modeling studies (Audiffren et al., 1999; Barth et al., 2001; Lawrence & Crutzen, 1998; Marécal et al., 2010; Mari et al., 2000; Neu & Prather, 2012). Removal of *stratospheric*  $\text{HNO}_3$  by convective ice scavenging, however, has yet to be observed and is currently hypothetical.

While stratospheric ozone recovery from the slow removal of inorganic chlorine from the stratosphere is expected to occur within this century driven largely by a decrease in ozone depleting substances (Austin et al., 2010; Chipperfield et al., 2017; Li et al., 2009; Oman & Douglass, 2014; Steinbrecht et al., 2018; Stone et al., 2018; World Meteorological Organization, 2014) due to the Montreal Protocol, recent modeling and observational studies show that additional halogen sources could slow this recovery (Engel et al., 2018; Hossaini et al., 2016; Yang et al., 2014). In particular, convectively transported halogenated very short lived substances of chlorine (Hossaini, Chipperfield, Montzka, et al., 2015; Hossaini, Chipperfield, Saiz-Lopez, et al., 2015; Hossaini et al., 2017; Laube et al., 2008; Oram et al., 2017), bromine (Aschmann et al., 2009; Dessens et al., 2009; Hossaini, Chipperfield, Montzka, et al., 2015; Liang et al., 2014; Salawitch et al., 2005; Wales et al., 2018; Yang et al., 2014), and iodine (Hossaini, Chipperfield, Saiz-Lopez, et al., 2015; Saiz-Lopez et al., 2015; Youn et al., 2010) have been shown to be important sources of stratospheric halogens. Further, both emissions of these halogenated very short lived substance (Ziska et al., 2017) and their transport to the stratosphere (Falk et al., 2017; Hossaini et al., 2012) are expected to increase with climate change resulting in a greater impact on stratospheric ozone (Fernandez et al., 2017; Tegtmeier et al., 2015). Therefore, while decreases in future stratospheric halogens may diminish the potential for convective water vapor enhancements and possible  $\text{HNO}_3$  removal to impact stratospheric ozone, convective perturbation may not become irrelevant for some time especially considering the importance of interhalogen reactions (e.g.,  $\text{ClO} + \text{BrO}$ ) to VSL-bromine contributions to ozone loss (Yang et al., 2014). Finally, despite potential recovery of upper stratosphere ozone, extrapolar lower stratosphere ozone has been declining since 1998 without an attributed cause (Ball et al., 2018). However, this trend has been disputed by analysis suggesting that the trend is not as significant when including the year 2017 and that ozone trends in the midlatitudes are largely due to dynamic variability (Chipperfield et al., 2018).

Previous studies have shown the potential for chlorine activation and ozone loss in the midlatitudes due to heterogeneous chemistry on cirrus cloud particles in the UTLS (Borrmann et al., 1996; Borrmann et al., 1997; Solomon et al., 1997). Many observations of elevated water vapor have been made in the midlatitudes lower stratosphere, however, in the absence of cirrus clouds (Hanisco et al., 2007; Hegglin et al., 2004; Randel et al., 2012; Ray et al., 2004; Smith et al., 2017; Weinstock et al., 2007). Additional studies then extended the sensitivity of the summertime Central United States lower stratospheric heterogeneous chlorine activation and ozone loss to water-sulfate aerosol surfaces resulting from such observed water vapor enhancements without cirrus cloud formation (Anderson et al., 2012; Anderson et al., 2017; Anderson & Clapp, 2018). Demonstrating potential chlorine activation on water-sulfate aerosols resulting from gaseous water vapor enhancements is significantly different from that on cirrus clouds because it greatly expanded the likelihood of chlorine activation in the midlatitudes due to the ubiquitous presence of sulfate aerosol in the lower stratosphere compared to the rarer cirrus clouds. Moreover, while cirrus clouds exist at altitudes at which there is little or no inorganic chlorine, sulfate aerosols are present at higher altitudes where there are greater background concentrations of inorganic chlorine (Solomon et al., 1997). Further, it demonstrated the possibility for observed gaseous water vapor enhancements to lead to chlorine activation and ozone loss within the convective outflow that remains coherent days after a convective event and in the absence of condensed water. These modeling studies of chlorine activation and ozone loss on water-sulfate aerosols at midlatitudes in the absence of cirrus clouds also detailed how that sensitivity depends on various stratospheric conditions that have a range of observed values, including temperature and background inorganic chlorine concentrations (Anderson et al., 2017; Anderson & Clapp, 2018).

In contrast, this paper aims to explore the sensitivity of lower stratospheric ozone to different properties of convective injection across the altitude-dependent chemical structure of the lower stratosphere. Specifically, while prior studies have demonstrated the effects of varying the magnitude of water vapor enhancements, the potential additional effect of convective perturbation,  $\text{HNO}_3$  scavenging, has not been explored. We use a photochemical box model to demonstrate the potentially exacerbating effect of convective  $\text{HNO}_3$  removal on ozone loss resulting from convectively injected water vapor enhancements. We also apply our

analysis across a vertical profile of physical and chemical conditions representative of the lower stratosphere (from 360- to 430-K potential temperature) to investigate the altitude dependence of  $\text{HNO}_3$  removal. We find column ozone loss of up to 1.5% after 7 days under perturbed conditions in the most extreme simulations with most initial conditions leading to column ozone loss of less than 1%. It should be noted that the results presented here represent a theoretical maximum chemical impact given the assumption of a coherent stratospheric air mass with convectively enhanced water vapor and/or nitric acid removal.

## 2. Methods

### 2.1. Model Description

We use a photochemical kinetics box model to explore the sensitivity of lower stratosphere chemistry to chemical and physical perturbations associated with convection as previously used in Anderson et al., 2012, and Anderson & Clapp, 2018. The chemical model tracks 32 chemical species and 67 reactions. Homogeneous and heterogeneous reactions and rate coefficients were taken from JPL (Sander et al., 2011) with daytime photolysis rates calculated using a fixed solar zenith angle of  $45^\circ$  and a radiative transfer model (Salawitch et al., 1994) representative of midlatitude summer conditions as per Anderson et al. (2012). Most important of these are the free radical cycles that destroy stratospheric ozone: the  $\text{HO}_x$ ,  $\text{NO}_x$ , and  $\text{ClO}_x$  cycles. The scope of vertical profile extends from 360- to 430-K potential temperature (approximately 14 to 18 km) with a resolution of 10 K. Each potential temperature level was simulated independently for a time period of up to 7 days using a range of initial conditions including differing water vapor concentrations, temperature profiles, and  $\text{HNO}_3$  concentrations. Analysis of cohesion of air masses within the lower stratospheric summertime anticyclone over the Central United States has shown lifetimes of up to 2 weeks (Koby, 2016). From the kinetics model, chemical concentrations for all the relevant species, including ozone, are calculated as a function of time per unit volume at each model level. The model state is defined by the chemical species number density and is integrated forward in time using the Livermore Solver for Ordinary Differential Equations with Automatic Switching ordinary differential equation solver. The model does not allow for advection, mixing, motion between levels, or radiative cooling.

To derive background concentrations of key chemical species used for model initialization, we define a box over the Central United States that extends from  $30^\circ$  to  $50^\circ\text{N}$  and  $110^\circ$  to  $80^\circ\text{W}$  as our region of interest. This box captures the region of most frequent, deep tropopause-penetrating convection as observed by NEXRAD (Cooney et al., 2018; D. L. Solomon et al., 2016) and is roughly coincident with the lower stratospheric North American Monsoon anticyclone. Chemical and physical properties used as inputs to the model are drawn from satellite or in situ observations made in this region during the summer months (June, July, and August) from 2004–2013. As little tropospheric mixing results from ice lofting, background stratospheric concentration profiles of  $\text{HCl}$ ,  $\text{HNO}_3$ ,  $\text{ClO}$ , and  $\text{O}_3$  were obtained from a decadal and regional average of Aura-MLS satellite data and used. The lowest level of 360 K was below the minimum level of  $\text{HCl}$  MLS data suggested for research use by MLS documentation and so was determined via extrapolation using a linear-logarithmic regression. Background profiles for  $\text{NO}_2$ ,  $\text{NO}$ , and inorganic bromine were obtained from in situ observations (Fahey et al., 1985; Ridley et al., 1994). The background profile for  $\text{BrO}$  was derived from a climatology of midlatitude summer stratosphere balloon measurements (Pundt et al., 2002). While using stratospheric chemical conditions as initial conditions after convective perturbation is a simplification of what is likely a complicated transport process, in situ stratospheric observations show convective water enhancements without tropospheric signal in carbon monoxide or ozone tracers, suggesting that this assumption does represent a potential outcome of convective transport (Frey et al., 2015; Phoenix et al., 2017).

To represent the range of observed convectively sourced humidity, we chose water vapor concentrations of 5, 10, 15, and 20 ppmv. The 5-ppmv simulations were used to represent background stratospheric water vapor mixing ratios. Midlatitude stratospheric water vapor concentrations are thought to be controlled primarily by the dehydration of ascending air through the cold-point tropopause during the Brewer-Dobson circulation (Butchart, 2014; Holton et al., 1995). Both model results and observations of the Brewer-Dobson control of midlatitude stratospheric water vapor have shown concentrations of around 5 ppmv (Fueglistaler et al., 2005; Ploeger et al., 2013; Schoeberl et al., 2012; Schoeberl & Dessler, 2011). The 10-, 15-, and 20-ppmv water vapor mixing ratio simulations were run to represent the range of observed convectively injected water vapor enhancements. In situ aircraft observations of elevated water vapor regularly reach 10-ppmv water vapor

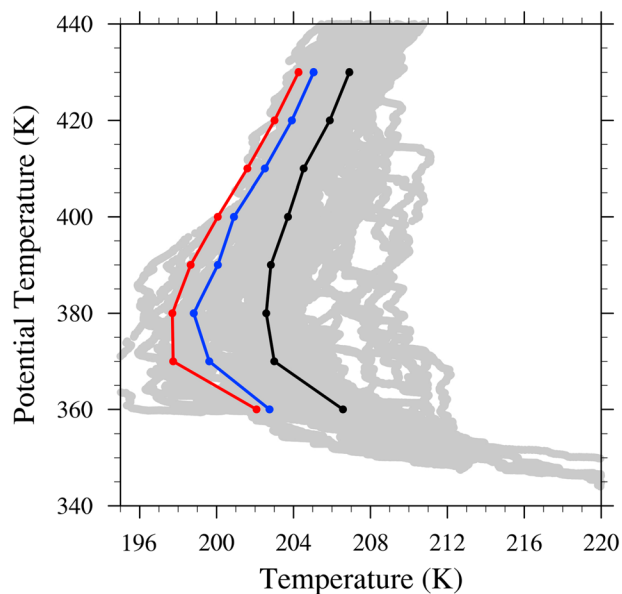


**Figure 2.** Studies of Emissions and Atmospheric Composition, Clouds, and Climate Coupling by Regional Surveys temperature observations in the previously defined region of interest and model temperature profiles. The average in each 10-K potential temperature bin is shown in black ( $T_{\text{avg}}$ ). The temperature halfway between  $T_{\text{avg}}$  and the minimum temperature in each 10-K potential temperature bin is shown in blue ( $T_{\text{mid}}$ ). The average of two minimum temperature profiles (in 10-K potential temperature bins) determined for data subselected to be from 30°N to 40°N and 40°N to 50°N is shown in red ( $T_{\text{min}}$ ).

with maxima of up to 18 ppmv (Anderson et al., 2017). Further, climate change is expected to increase the frequency and intensity of deep convection over the Central United States and therefore the likelihood of convective hydration (Diffenbaugh et al., 2013; Feng et al., 2016; Trapp et al., 2009). In the simulations in which the temperature profiles resulted in instances of water vapor concentrations above the saturation mixing ratio, water vapor was allowed to remain supersaturated for 1 day before being pinned to the saturation mixing ratio.

Three temperature profiles were used to cover the range of temperatures observed in the lower stratosphere over the Central United States during summer. Temperature at each potential temperature level was held constant throughout the entire simulation. These profiles are shown in Figure 2. Temperatures tend to increase with increasing altitude that decreases the probability of chlorine activation at higher potential temperature surfaces due to the probability of the heterogeneous reactions being favored by colder conditions. The temperatures were taken from the National Aeronautics and Space Administration (NASA) Studies of Emissions, Atmospheric Composition, Clouds, and Climate Coupling by Regional Surveys (SEAC<sup>4</sup>RS) ER-2 flight data. The ER-2 flew over the Central United States during the summer of 2013 (Toon et al., 2016). From the temperature data available, measured with the Meteorological Measurement System (Scott et al., 1990), only data within the region of interest were used. The first profile, the average temperature ( $T_{\text{avg}}$ ) was selected to provide a baseline. The average was calculated by averaging the data over 10-K potential temperature bins centered on each isentropic level considered in the photochemical model. The second, a colder pseudo-minimum tempera-

ture profile ( $T_{\text{min}}$ ) was constructed to capture the large variance in temperature observed. Due to the latitudinal differences in temperature, taking the absolute minimum of the complete data set would only represent the coldest region of the area of interest and introduce a latitude bias. Therefore, the two minimum temperature profiles for the data within 30°N to 40°N and 40°N to 50°N were averaged to more accurately represent the colder temperatures across the entire domain. A curve defined as the average between the average and the minimum ( $T_{\text{mid}}$ ) is also used to demonstrate the remarkable non-linear sensitivity of the system to relatively small changes in background stratospheric temperatures. For additional information on the photochemical model including reactions and initial conditions for key chemical species, refer to the supporting information.

Observations of the efficiency of  $\text{HNO}_3$  removal by ice include a wide range from several percent removal to complete removal depending on factors such as temperature, particle size, and partial pressure (Abbatt, 1997; Krämer et al., 2008; Mari et al., 2000). To explore the sensitivity of chlorine activation and stratospheric ozone to this potential process for different efficiencies of  $\text{HNO}_3$  removal, simulations were run with 5%, 10%, 20%, 30%, 50%, 70%, and 100% removal of the initial  $\text{HNO}_3$ .

The background sulfate aerosol SAD of  $2 \mu\text{m}^2/\text{cm}^3$  was taken from a SAGE satellite climatology for the latitude (30–50°N) and altitude (14–18 km) region of interest (Thomason et al., 1997). An elevated aerosol SAD of  $6 \mu\text{m}^2/\text{cm}^3$  was selected to represent an enhancement from volcanic activity or potential SRM. For reference, the enhancement to sulfate aerosol SAD in the Northern Hemisphere midlatitudes from the Pinatubo eruption reached maxima as high as  $20 \mu\text{m}^2/\text{cm}^3$  and for the El Chichon eruption as high as  $10 \mu\text{m}^2/\text{cm}^3$  (Fahey et al., 1993; Hofmann & Solomon, 1989; S. Solomon et al., 1996; Thomason et al., 1997; Wilson et al., 1993).

## 2.2. Initial Conditions

To differentiate the additional effects of convective  $\text{HNO}_3$  removal on chlorine activation and ozone loss from the effects of convective water vapor enhancements, a set of 24 simulations were performed with

the background  $\text{HNO}_3$  profile as controls. The control simulations include all four initial water vapor concentrations (5, 10, 15, and 20 ppmv) over each temperature profile ( $T_{\text{avg}}$ ,  $T_{\text{mid}}$ , and  $T_{\text{min}}$ ) for both 2- and  $6\text{-}\mu\text{m}^2/\text{cm}^3$  sulfate aerosol SAD.

To test the effects of a range of potential convective  $\text{HNO}_3$  removal efficiencies, each of the above 24 water vapor concentration, temperature profile, and sulfate aerosol SAD initial condition combinations were simulated with 0%, 30%, 50%, 70%, 80%, 90%, and 95% of the initial background  $\text{HNO}_3$ .

### 3. Results

#### 3.1. Control Simulations: Varied Water Vapor and Temperature

To parse the impact of potential convective  $\text{HNO}_3$  removal on the chemical composition of the lower stratosphere from the impact of convective water vapor enhancements, a brief analysis of the control simulations is necessary. From the control simulations, (1) the chemical mechanism that translates water vapor enhancements to chlorine activation and ozone loss can be identified, (2) the effects of different temperature profiles interacting with water vapor enhancements can be demonstrated, and (3) the cumulative result of competing trends in the vertical distributions of inorganic chlorine, ozone, and  $\text{NO}_y$  (total reactive nitrogen including  $\text{NO}_x$ ,  $\text{HNO}_3$ ,  $\text{N}_2\text{O}_5$ ,  $\text{NO}_3$ , and  $\text{HONO}$ ) on chlorine activation and ozone loss can be summarized. How  $\text{HNO}_3$  removal interacts with this chemical mechanism, particularly during the first 2 days following convective injection during which the majority of chlorine activation occurs, determines how it can potentially exacerbate convective perturbations to the lower stratosphere including under meteorological conditions and at what altitudes it has the greatest impact.

The chemical mechanism that leads to chlorine activation and ozone loss is driven by the heterogeneous chlorine activation reactions (R9–R11). These reactions lead to a series of subsequent chemical effects that result in a sequential transformation of the chemical composition of the lower stratosphere. Figure 3 shows both how the heterogeneous chlorine activation reactions drive a series of chemical changes and the dependence of these reactions on water vapor. Figure 3a shows the chemical concentrations of key species that are relevant to chlorine activation as a function of time for the stratospheric background mixing ratio (5 ppmv) of initial water vapor at  $T_{\text{mid}}$ . Under these conditions, the heterogeneous reactions have minimal effect on the chemical composition of the lower stratosphere. Over the course of 120 hr only approximately 12% of initial  $\text{NO}_x$  is converted to  $\text{HNO}_{3(\text{aq})}$  (all nitric acid is initialized in the gas phase), and therefore, no significant chlorine activation occurs: All of the inorganic chlorine is present in the reservoir chlorine species of  $\text{HCl}$  and  $\text{ClONO}_2$ , and the dominant chemical feature is the diurnal cycle between  $\text{NO}$  and  $\text{NO}_2$ . In contrast, Figure 3b shows the response of the chemical concentrations of key species relevant to chlorine activation as a function of time for 10 ppmv of initial water vapor at  $T_{\text{mid}}$ , conditions that favor significant chlorine activation. The chlorine activation mechanism can be divided into two phases. In the first phase (until 14 hr in Figure 3b), in which  $\text{NO}_x$  is present, reservoir inorganic chlorine is repartitioned from  $\text{HCl}$  to  $\text{ClONO}_2$  concurrent with conversion of  $\text{NO}_x$  to aqueous  $\text{HNO}_3$ . In the second phase (hours 14 through 38 in Figure 3b), with  $\text{NO}_x$  depleted, reservoir inorganic chlorine is converted to free radical chlorine and gaseous nitric acid increases as it equilibrates aqueous nitric acid. After the second phase, an equilibrium is approached over the subsequent days in which the inhibitory effect of  $\text{NO}_x$  regeneration by  $\text{HNO}_3$  photolysis on chlorine activation equals the rate of chlorine activation by the heterogeneous reactions. In this equilibrium, the diurnal cycle dictates which chlorine species are present.

The above chemical changes are driven by the heterogeneous chlorine activation reactions. The products of the heterogeneous chlorine activation reactions,  $\text{Cl}_2$  and  $\text{HOCl}$ , rapidly photolyze to free radical chlorine which will react with  $\text{O}_3$  to form  $\text{ClO}$ .  $\text{ClO}$  will then react with  $\text{NO}_2$  to form  $\text{ClONO}_2$  or with  $\text{NO}$  to form  $\text{Cl}$  and  $\text{NO}_2$ . As a result, in the first phase, these reactions cycle chlorine through  $\text{ClO}$  from  $\text{HCl}$  to  $\text{ClONO}_2$  while converting  $\text{NO}_x$  to  $\text{HNO}_{3(\text{aq})}$ . With  $\text{NO}$  and  $\text{NO}_2$  depleted in the second phase, reactive chlorine species (such as  $\text{ClO}$ ,  $\text{ClOOCl}$ , and  $\text{Cl}_2$ ) can emerge as a major category of inorganic chlorine. Also, beginning in the second phase and continuing onward,  $\text{HNO}_3$  oscillates diurnally as  $\text{HNO}_{3(\text{aq})}$  returns to the gas phase resulting in increases at night but is lost to photolysis during the day to regenerate  $\text{NO}_x$ . This in turn results in an oscillation of about 10–20% of the  $\text{ClO}$  generated in the second phase due to deactivation by reaction with  $\text{NO}_2$  to reform  $\text{ClONO}_2$  during the day and reactivation during the night when the

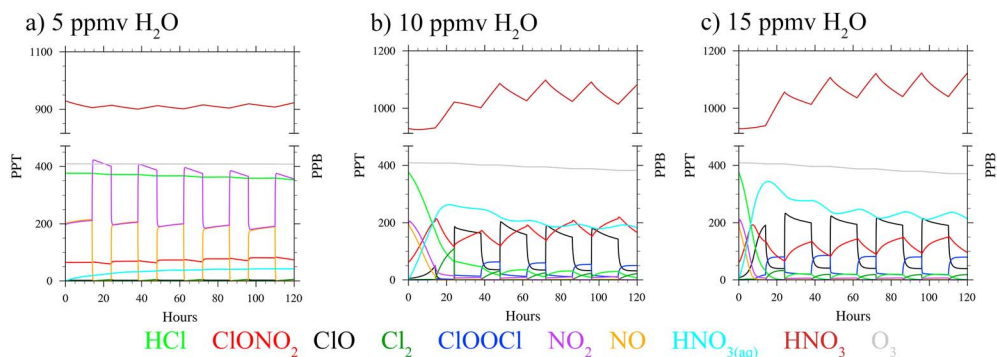


**Figure 3.** (a) Concentrations of key chemical species including reservoir chlorine (HCl and ClONO<sub>2</sub>), free radical chlorine (Cl<sub>2</sub>, ClO, and ClOOCl), NO<sub>x</sub> (NO<sub>2</sub> and NO), aqueous and gaseous nitric acid, and ozone as a function of time from the  $T_{\text{mid}}$  and 5-ppmv water vapor (background) simulation at 380 K. Ozone is shown in units of parts per billion (PPB) by volume (right axis) and all other species are in units of parts per trillion (PPT) by volume (left axis). (b) Chemical concentrations as in (a) but for 10 ppmv of water vapor. The changes in chemical composition are driven by the heterogeneous chlorine activation reactions. (c) Chemical concentrations as in (b) but for 15 ppmv of water vapor.

heterogeneous reactions dominate (which also drives HNO<sub>3</sub> increases at night through the production of HNO<sub>3(aq)</sub>). After the second phase free radical chlorine catalytically destroys ozone resulting in a loss over the subsequent days as long as the heterogeneous reactions are favored and maintain the elevated free radical chlorine concentration.

The heterogeneous chlorine activation mechanism is strongly dependent on the uptake of the chlorine reactants of HCl, ClONO<sub>2</sub>, and HOCl onto sulfate aerosols and therefore on water vapor concentration and temperature. Both cold temperatures and high humidity favor chlorine activation on sulfate aerosols and subsequent ozone loss. Figure 3c shows a time series of concentrations of chemical species that are relevant to chlorine activation as in Figure 3a but at 15 ppmv of water vapor. The effect of higher humidity on the chlorine activation chemical mechanism can be seen in the inorganic chlorine repartitioning, NO<sub>x</sub> loss, and free radical chlorine accumulation, which are faster and in greater magnitude as compared to Figure 3b. More generally, Figure 4a shows the impact of increasing water vapor concentrations in the control simulations on the resulting ozone loss between 360 and 430 K after 7 days of elevated water vapor for all three temperature profiles. Increasing initial water vapor concentrations increases the amount of ozone loss, but the effect is not linear. Within each temperature profile the nonlinearity of the sensitivity to water vapor concentration resulted in sharp transitions of the simulation from the unperturbed stratospheric state, with little to no ozone loss, to the ozone loss state. Where that transition point fell with respect to water vapor concentration was dependent on the chosen temperature profile. For the  $T_{\text{min}}$  temperature profile, the greatest response in ozone loss after 7 days under perturbed conditions to water vapor concentration increases comes at the 10-ppmv value. For the  $T_{\text{mid}}$  profile the transition was smoothest, but with the largest increase occurring at 15 ppmv of water vapor, and for the  $T_{\text{avg}}$  profile the largest increase occurred at 20 ppmv of water vapor. These transition points correspond to a range of water vapor concentrations in which the uptake probability and rate of chlorine activation rapidly rises from near zero to its maximum, beyond which additional water vapor only results in marginal increase as the uptake probability as the uptake probability and rate of chlorine activation have largely reached a maximum. To illustrate, Figure 4b shows the dependence of the reaction rate of HCl with ClONO<sub>2</sub> (R9) on water vapor concentration for the three temperature profiles in which the regions of rapid increase in rate with respect to water vapor concentration correspond to the ozone loss increases in Figure 4a. At colder temperatures this range occurs at lower water vapor concentrations and the range of rapid increase is narrower, which exacerbates the sensitivity of the heterogeneous reactions to humidity. In summary, due to the nonlinearity of the dependence of the reaction rates of heterogeneous chlorine activation on uptake probability, there is a threshold of water vapor concentration that corresponds to a rapid increase in chlorine activation and ozone loss. This threshold is temperature dependent with colder temperatures having lower water vapor thresholds.

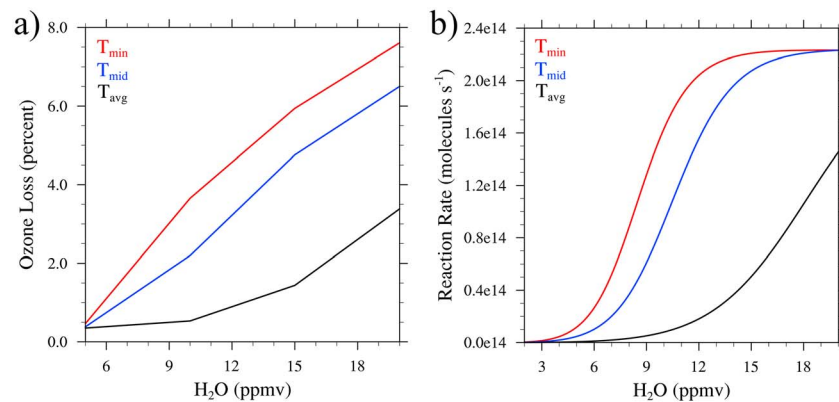


**Figure 4.** (a) The total percent ozone loss after 7 days between 360 and 430 K for each temperature profile as a function of initial water vapor concentration (ppmv), illustrating the nonlinearity of response to initial conditions. (b) The rate of  $\text{ClONO}_2 + \text{HCl} \rightarrow \text{Cl}_2 + \text{HNO}_3$  as a function of water vapor concentration at the average temperature and pressure for 370–390 K for each of the three temperature profiles:  $T_{\text{avg}}$  (203.7 K and 119.4 hPa),  $T_{\text{mid}}$  (200.3 K and 112.4 hPa), and  $T_{\text{min}}$  (199.0 K and 110 hPa). The rapid increase in rate occurs in different ranges of water vapor for each temperature profile.

For analysis of the net effect of chemically relevant competing vertical trends (temperature, background inorganic chlorine mixing ratio, background ozone concentration, and background reactive nitrogen) on the chlorine activation mechanism across the vertical range of 360–430 K, we plot the sum of the concentrations of three categories of chemical species in our figures that utilize the vertical coordinate as the y axis for ease of visual assessment. These categories include total inorganic reservoir chlorine (HCl and  $\text{ClONO}_2$ ), reactive chlorine that includes free radical chlorine and its sources (Cl, ClO,  $\text{Cl}_2$ , ClOOCl, and HOCl), and  $\text{NO}_x$  (NO and  $\text{NO}_2$ ). By plotting the simulation results with these three chemical categories the sequential effects of the chlorine activation chemical mechanism are captured with less visual complexity across the vertical dimension. Figure 5a shows a time series of the categories of chemical concentrations for 10 ppmv of water vapor and Figure 5b for 15 ppmv of water vapor at  $T_{\text{mid}}$ . Comparison with Figure 3 demonstrates the capability of the simplified set of chemical concentrations to represent the chlorine activation chemical mechanism. The concentration of  $\text{NO}_x$  tracks the progress of the first phase of the chemical mechanism. The rapid decrease in  $\text{NO}_x$  from simulation initiation to 14 hr captures the effect of the first phase of the chlorine activation chemical mechanism because it is the net result of inorganic chlorine being repartitioned from HCl to  $\text{ClONO}_2$  through cycling of ClO, which reacts with  $\text{NO}_2$  to ultimately convert  $\text{NO}_x$  to  $\text{HNO}_{3(\text{aq})}$ . The decreasing concentration of reservoir chlorine and corresponding increasing reactive chlorine track the progress of the second phase of the chemical mechanism (after 14 hr of simulation) in which, in the absence of  $\text{NO}_x$ , reservoir chlorine is not repartitioned by the heterogeneous chlorine reactions but is converted to reactive chlorine. In the context of the vertically varying stratospheric background conditions, reservoir chlorine profiles show the effect of the heterogeneous reactions as they relate to its background vertical gradient, while reactive profiles illustrate the overall effect of the competing vertical effects on the amount of chlorine activated at each potential temperature level.

Figure 6 shows the result of the competing factors on the vertical chemical structure of the lower stratosphere in response to a convective perturbation in water vapor. The figure illustrates the effect of the 10 ppmv of water vapor control simulation as a function of time for all three temperature profiles. The times of 6, 12, and 36 hr show the progression from an unperturbed chemical state to an ozone loss state: 6 hr shows the initial reaction, 12 hr shows the intermediate progression for a comparison of rates under different conditions, and by 36 hr the final result of the chemical transition is evident as most of the chlorine activation has occurred by this time. The first large deviation from background concentrations is evident in the decrease in the  $\text{NO}_x$  profile at 6 hr for  $T_{\text{mid}}$  and  $T_{\text{min}}$ , which is followed by the subsequent loss of reservoir chlorine and an increase in free radical chlorine by 36 hr. Within the vertical structure of these profiles, the dependence of the chlorine activation chemical mechanism on temperature had the strongest influence: The potential temperature level with the coldest temperatures, 380 K, has the fastest and largest chemical response. Depending on the temperature profile, 380 K showed the most consistent, nearly complete  $\text{NO}_x$

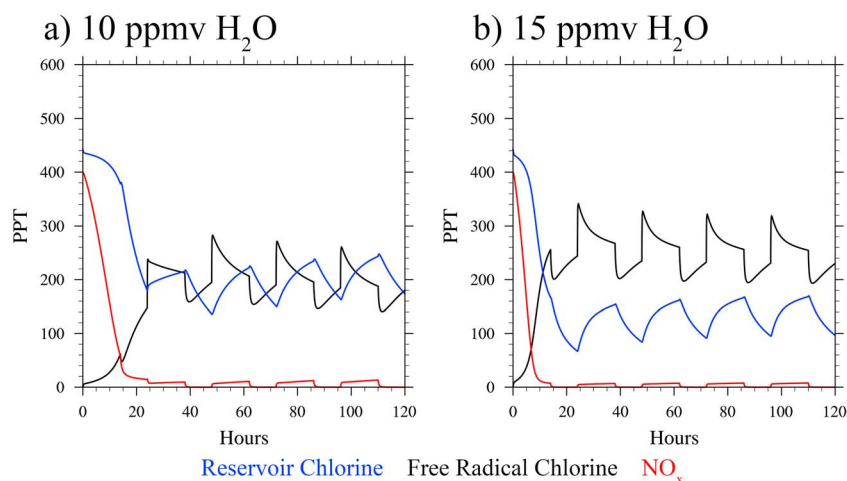


**Figure 5.** (a) Concentrations of key chemical species combined into simplified categories ( $\text{HCl}$  and  $\text{ClONO}_2$ ), free radical chlorine ( $\text{Cl}_2$ ,  $\text{ClO}$ ,  $\text{Cl}$ ,  $\text{HOCl}$ , and  $\text{ClOOCl}$ ), and  $\text{NO}_x$  ( $\text{NO}_2$  and  $\text{NO}$ ) as a function of time from the  $T_{\text{mid}}$  and 10-ppmv water vapor simulation at 380 K. (b) Simplified chemical concentrations as in (a) but for 15 ppmv of water vapor. PPT = parts per trillion.

depletion at  $T_{\text{mid}}$  and  $T_{\text{min}}$ , with 390 and 370 K also being cold enough for significant loss at  $T_{\text{min}}$ . The effect of the vertical gradient in  $\text{HCl}$  becomes evident for the simulation with  $T_{\text{min}}$ . By 36 hr, reservoir chlorine and free radical chlorine profiles at 390 K show greater chlorine activation than at 370 K despite similar amounts of, and even faster  $\text{NO}_x$  depletion, at 370 K. Finally, the increasing concentration of background ozone with altitude results in the small free radical chlorine concentrations at upper levels leading to larger relative ozone loss. At 410 K, approximately a tenth of the free radical chlorine at 370 K led to approximately a fourth of the ozone loss.

With the above context of the dependence of the chlorine activation chemical mechanism on both enhanced humidity from convective transport and stratospheric temperature and on the vertical profiles in the lower stratosphere in temperature, inorganic chlorine, ozone, and reactive nitrogen, demonstrated by the control simulations, in the following section we present the results of potential  $\text{HNO}_3$  removal by convection. We describe (1) the effect of  $\text{HNO}_3$  on the chlorine activation chemical mechanism, (2) the dependence of the  $\text{HNO}_3$  removal effect on initial conditions relevant to chlorine activation, and (3) the effect of the magnitude of  $\text{HNO}_3$  removal on chlorine activation and ozone loss across the vertical structure of the lower stratosphere. We then examine how the effect of  $\text{HNO}_3$  removal changes under higher sulfate aerosol SAD conditions.

### 3.2. $\text{HNO}_3$ Removal Simulations

$\text{HNO}_3$  interacts with the chlorine activation chemical mechanism by acting as a reservoir for the  $\text{NO}_x$  species. In the control simulations, the photolysis of  $\text{HNO}_3$  to form  $\text{OH}$  and  $\text{NO}_2$  acted as a source of  $\text{NO}_x$ . Similarly, the reaction of  $\text{HNO}_3$  with  $\text{OH}$  to form  $\text{H}_2\text{O}$  and  $\text{NO}_3$ , which would subsequently photolyze to form  $\text{NO}$ , was also a  $\text{NO}_x$  source. As a result, removal of initial  $\text{HNO}_3$  removes a source of  $\text{NO}_x$ . Figure 7 shows the effect of  $\text{HNO}_3$  removal on the contribution of  $\text{NO}_x$  production as a function of percent  $\text{HNO}_3$  removal resulting from the above reactions during the two phases of chlorine activation. As more  $\text{HNO}_3$  is removed,  $\text{NO}_x$  production slows, and less  $\text{NO}_x$  is available from these reactions. To illustrate the effect of lower  $\text{NO}_x$  on the overall chlorine activation chemical mechanism, Figure 8a shows a time series of key chemical species relevant to chlorine activation for a simulation with 30% removal of initial  $\text{HNO}_3$  and Figure 8b shows the anomalies for these chemical species as compared to the corresponding control simulation. In the figure, while the conversion of  $\text{NO}_x$  to  $\text{HNO}_{3(\text{aq})}$  of the first phase of the chemical mechanism occurs at approximately the same rate, without  $\text{HNO}_3$  as a  $\text{NO}_x$  source, lower concentrations of  $\text{NO}_x$  are available to the system (5.3 pptv compared to 9.3 pptv) during the second phase of the mechanism in which reservoir inorganic chlorine is converted to free radical chlorine. As a result, more overall chlorine activation

10 ppmv H<sub>2</sub>O 2 μm<sup>2</sup>cm<sup>-3</sup>

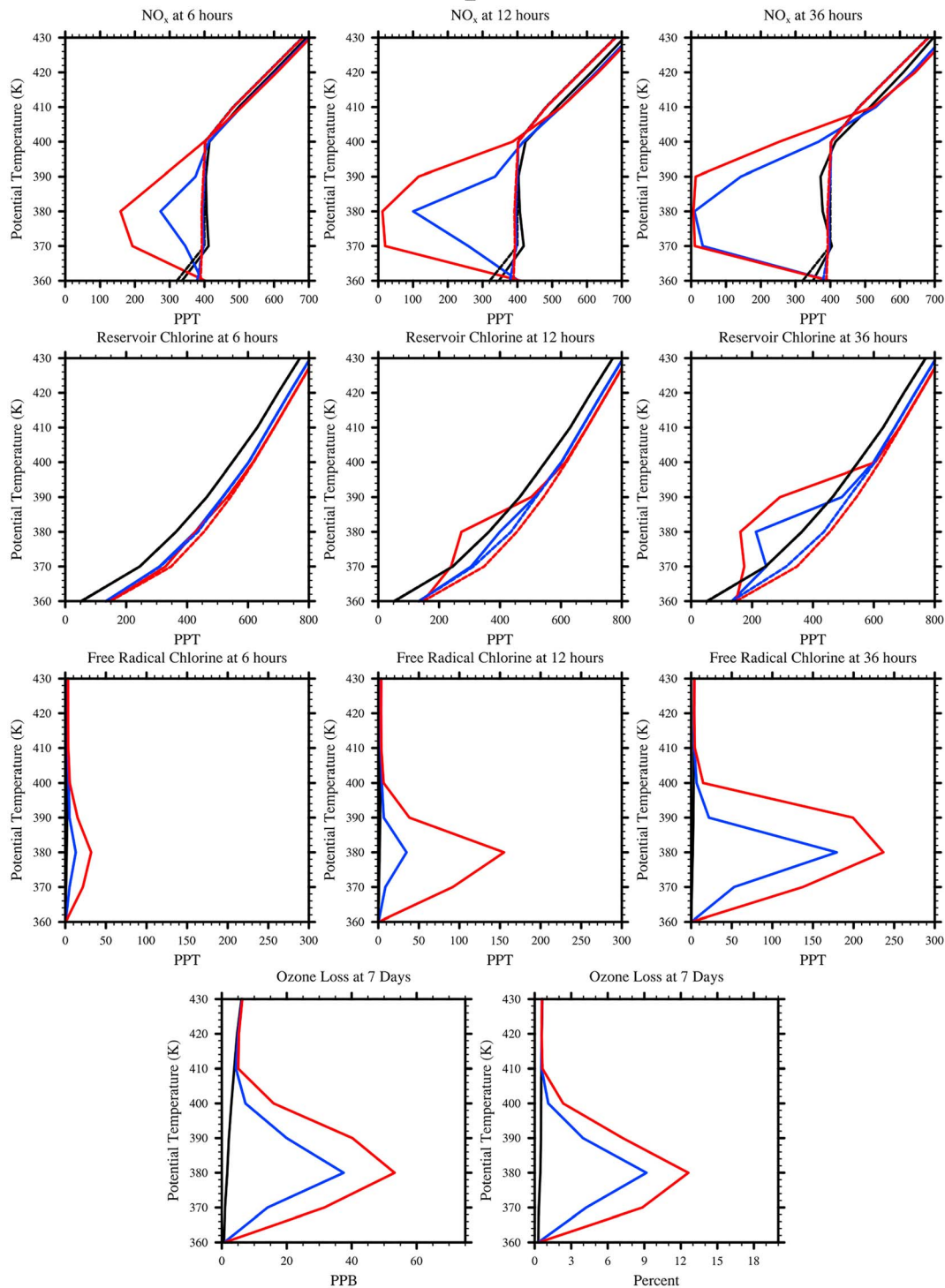


**Figure 6.** Vertical profiles of key chemical species (NO<sub>x</sub> in the first row, reservoir chlorine in the second row, and free radical chlorine in the third row) that track the sequence of changes to the chemical structure of the lower stratosphere over time from 6 to 12 and 36 hr. Shown here are results for 10 ppmv of water vapor and 2-μm<sup>2</sup>/cm<sup>3</sup> sulfate aerosol surface area density at all three temperature profiles (T<sub>avg</sub> in black, T<sub>mid</sub> in blue, and T<sub>min</sub> in red). Initial concentrations are indicated by the dashed lines. By 36 hr, the majority of chlorine activation has occurred. The effect of chlorine activation through the heterogeneous reactions first manifests in decreases in NO<sub>x</sub> (NO and NO<sub>2</sub>) followed by a partial conversion of reservoir chlorine (HCl and ClONO<sub>2</sub>) to free radical chlorine (Cl, ClO, ClOOCl, and Cl<sub>2</sub>) over time. Finally, vertical profiles of ozone loss in parts per billion by volume and percent after 7 days of perturbed conditions are shown, summarizing the impact of chlorine activation. PPT = parts per trillion.

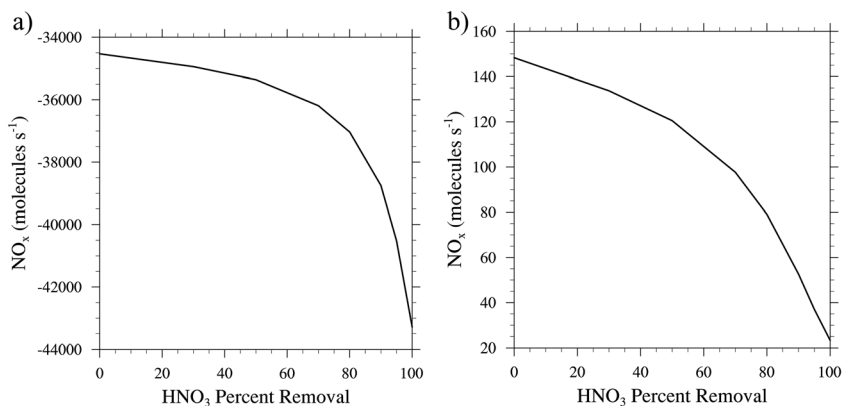


**Figure 7.** (a) The effect of nitric acid removal on  $\text{NO}_x$  depletion during the first phase of the chlorine activation chemical mechanism shown by the rate of change of  $\text{NO}_x$  ( $\text{NO}_2 + \text{NO}$ ) concentration as function of initial  $\text{HNO}_3$  removal percent at 30 min for at the 380-K level with 15 ppmv of water vapor at  $T_{\text{mid}}$  and (b) on  $\text{NO}_x$  sources during the second phase of free radical chlorine accumulation at 30 hr, also at 380 K with 15 ppmv of water vapor at  $T_{\text{mid}}$ .

occurred as demonstrated by the higher concentrations of  $\text{ClO}$  present after activation has occurred (183 pptv compared to 166 pptv in the control) instead of being diverted to the repartitioning of  $\text{HCl}$  to  $\text{ClONO}_2$ .

The overall impact of  $\text{HNO}_3$  removal on the chlorine activation chemical mechanism via eliminating a  $\text{NO}_x$  source was dependent on the initial temperature and water vapor conditions as well as the vertical profiles of temperature and key chemical species. Because  $\text{HNO}_3$  primarily interacts with chlorine activation by providing a source of  $\text{NO}_x$  that will divert  $\text{ClO}$  to  $\text{ClONO}_2$ , the loss of a potential  $\text{NO}_x$  source is only significant under conditions in which  $\text{ClO}$  production through the heterogeneous chlorine reactions are favored. As a result, a given reduction of initial  $\text{HNO}_3$  had a greater impact on simulations with lower temperatures and higher initial water vapor concentrations as well as at upper levels in which more inorganic chlorine is available. To illustrate this scaling of the impact of initial  $\text{HNO}_3$  removal on the favorability of the heterogeneous reactions, Figure 9 shows the vertical profiles of the simplified chemical species ( $\text{NO}_x$ , inorganic reservoir chlorine, and reactive chlorine) that summarize the progress of the chlorine activation chemical mechanism for 30% removal of initial  $\text{HNO}_3$  at 10 ppmv of water vapor for all three temperature profiles. The solid lines show the  $\text{HNO}_3$  removal simulation results, and the dashed lines show the results for the corresponding control simulation. Simulations with colder temperatures result in a greater amount of overall chlorine activation as shown by greater values of reactive chlorine at 36 hr in both the colder temperature profiles ( $T_{\text{mid}}$  and  $T_{\text{min}}$ ) and the colder potential temperatures (370–390 K). In contrast, simulations with warmer temperatures show an insensitivity to  $\text{HNO}_3$  removal, as can be seen in figure in which the

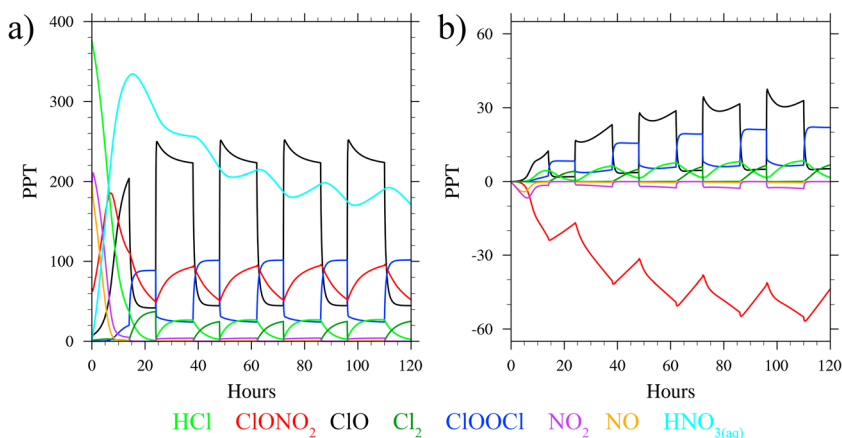


**Figure 8.** (a) As in Figure 3 but with 30% initial  $\text{HNO}_3$  removal for 15 ppmv of water vapor at  $T_{\text{mid}}$ . (b) Concentration anomalies as compared to the control simulation in Figure 3. PPT = parts per trillion.

### 30% HNO<sub>3</sub> Removal 10 ppmv H<sub>2</sub>O 2 μm<sup>2</sup>cm<sup>-3</sup>

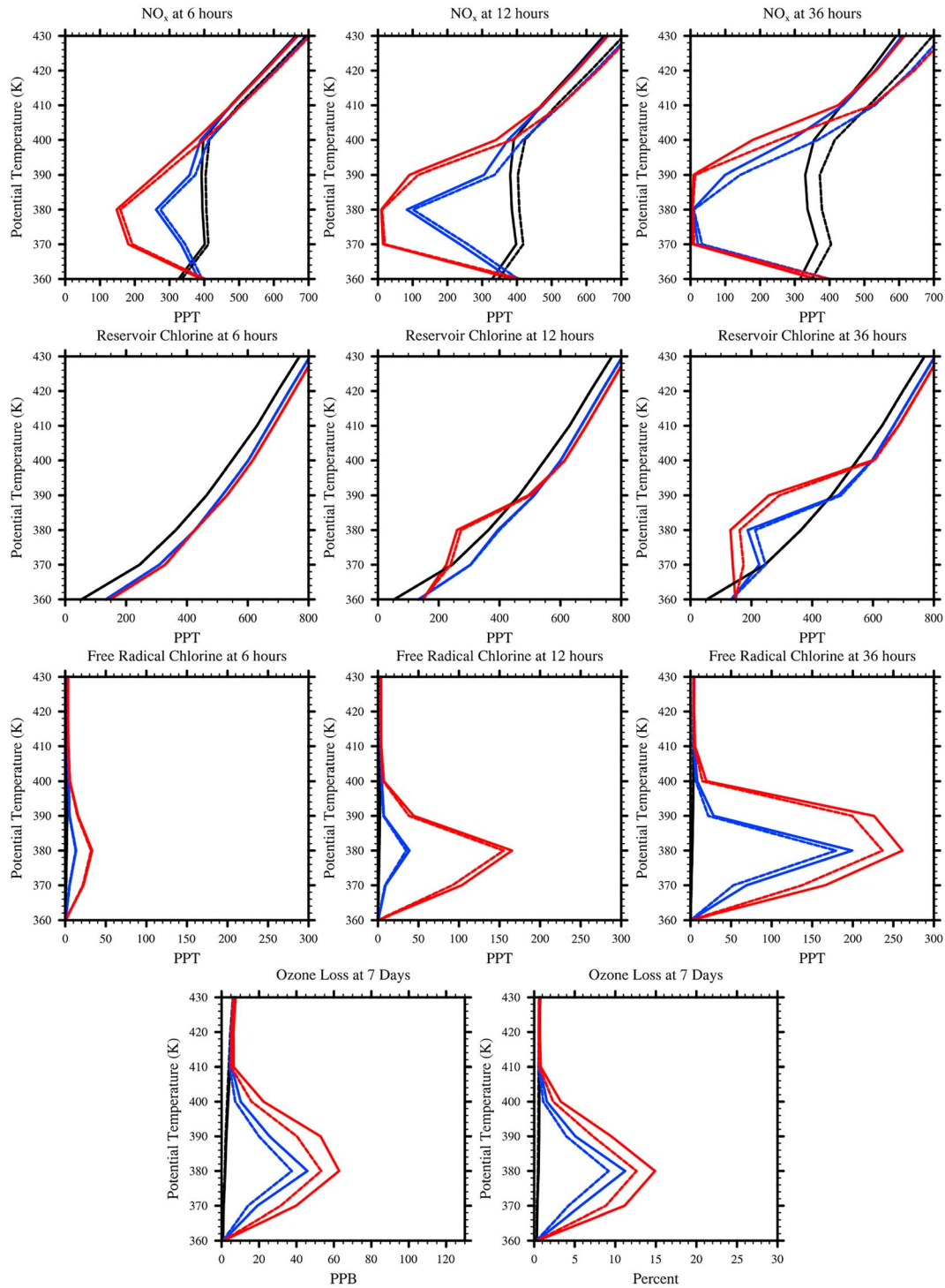


**Figure 9.** To show the effect of 30% initial HNO<sub>3</sub> removal, vertical profiles of key chemical species as in Figure 6 are shown here for 10 ppmv of water vapor and 2-μm<sup>2</sup>/cm<sup>3</sup> sulfate aerosol surface area density. Vertical profiles of each species for the corresponding control simulation with 10 ppmv of water vapor and no initial nitric acid removal are shown by the dashed lines for comparison. PPT = parts per trillion.

### 30% HNO<sub>3</sub> Removal 15 ppmv H<sub>2</sub>O 2 μm<sup>2</sup>cm<sup>-3</sup>

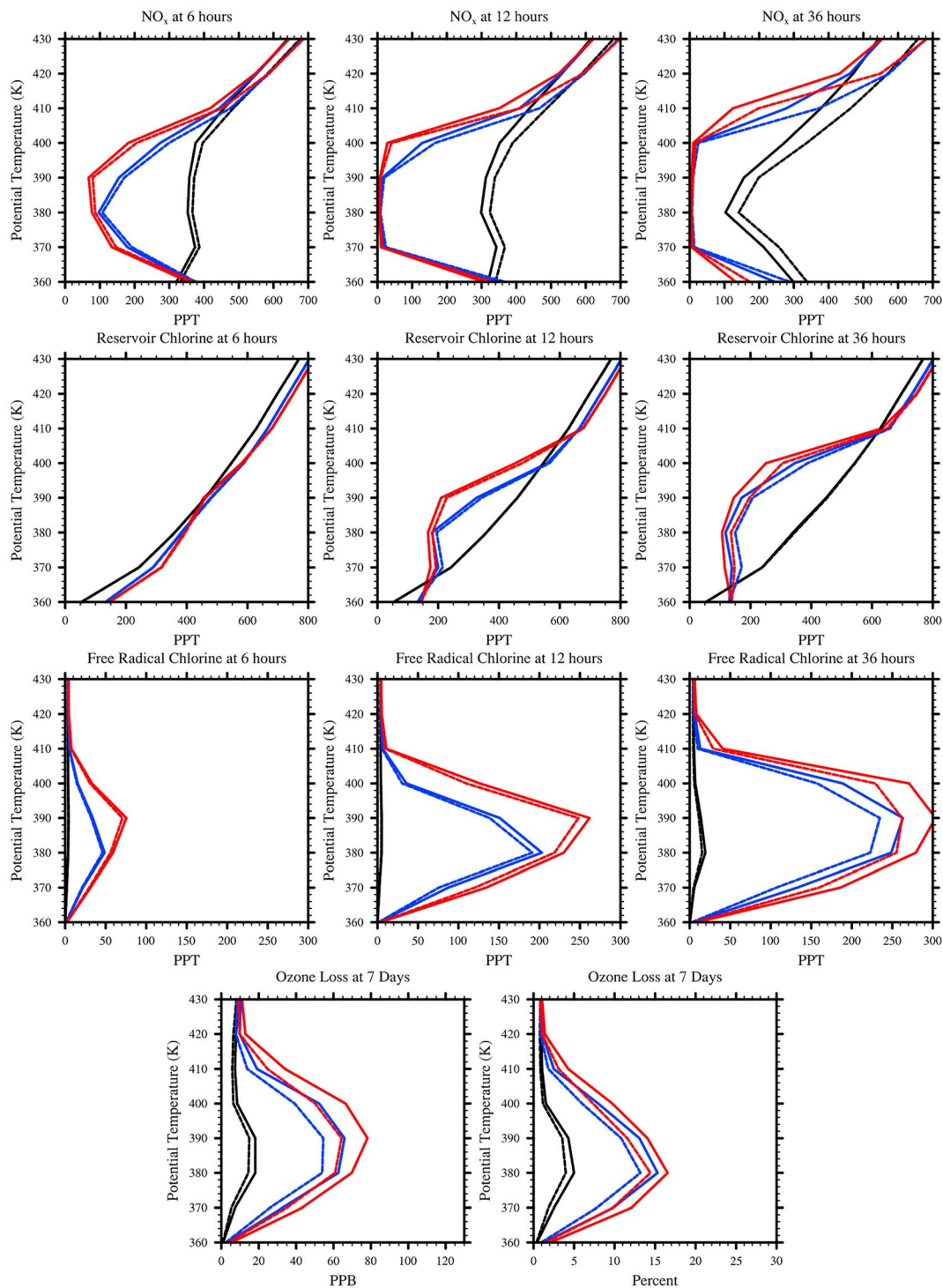


**Figure 10.** As in Figure 9 but with 15 ppmv of water vapor. PPB = parts per billion; PPT = parts per trillion.

HNO<sub>3</sub> removal resulted in no additional reactive chlorine at 36 hr at the potential temperatures of 360 and 410–430 K, because the heterogeneous reactions that generate free radical chlorine are not favored at these temperatures. With 15 ppmv of initial water vapor, as shown by the vertical profiles in Figure 10, the same 30% removal of initial HNO<sub>3</sub> resulted in higher concentrations of reactive chlorine at 36 hr at all levels with

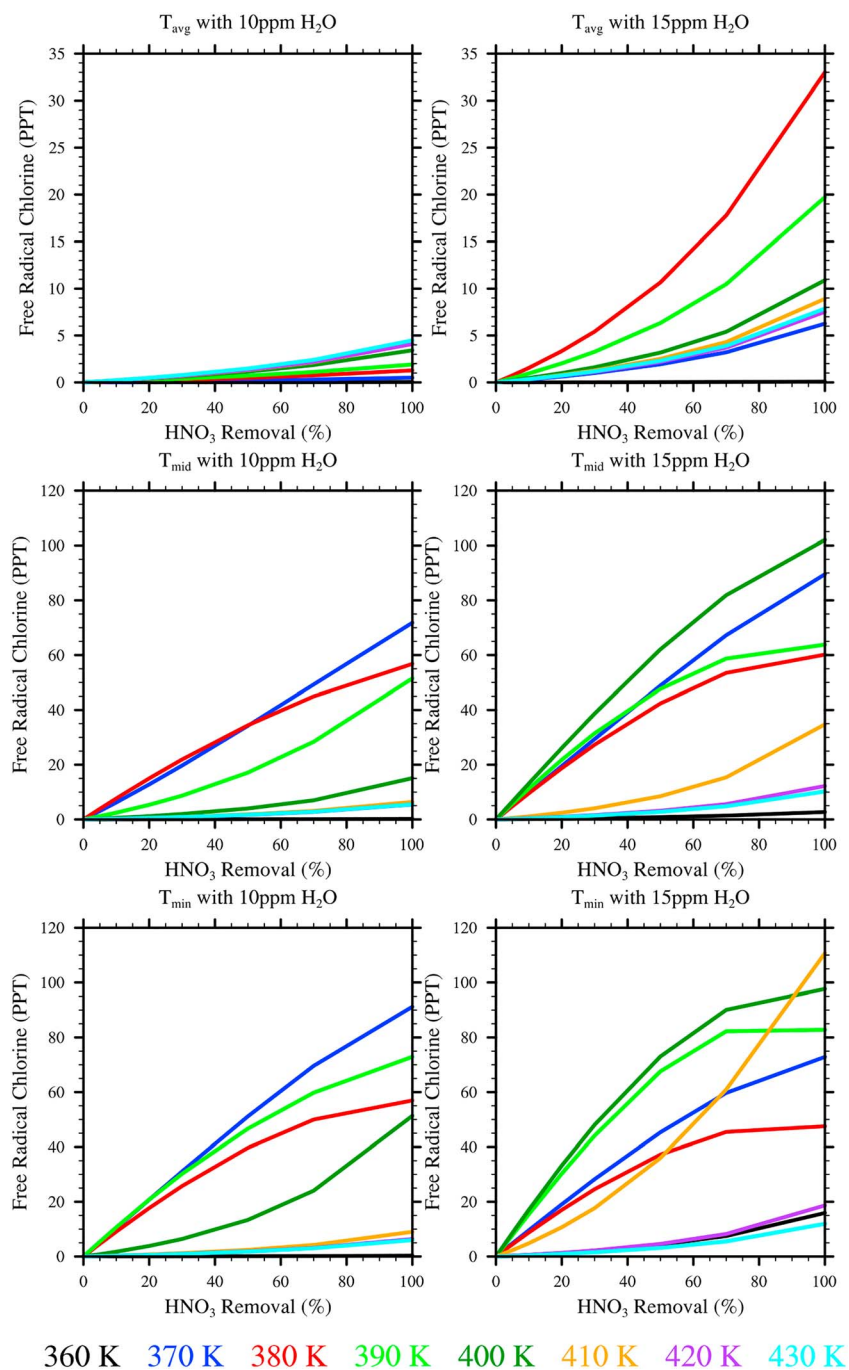


**Figure 11.** Each panel shows the increases in the concentration of free radical chlorine compared to control simulations resulting from nitric acid removal after simulated 36 hr of elevated water vapor as a function of initial HNO<sub>3</sub> percent removal at all eight potential temperatures (indicated by color) within a simulation. Shown are the simulations with 10 and 15 ppmv of water vapor for  $T_{avg}$ ,  $T_{mid}$ , and  $T_{min}$ . PPT = parts per trillion.

significant chlorine activation than with 10 ppmv of initial water vapor. Also in Figure 10, the vertical effect of the background inorganic chlorine concentration that increases with altitude is shown by the largest increases in reactive chlorine concentration at 36 hr due to HNO<sub>3</sub> removal occurring at 390 and 400 K. The effect of HNO<sub>3</sub> removal on the chlorine activation mechanism requires initial conditions that independently favor chlorine activation (low temperatures and high humidity). Further, the impact of the same amount of HNO<sub>3</sub> removal on chlorine activation becomes greater in magnitude as the initial conditions become more favorable to chlorine activation.

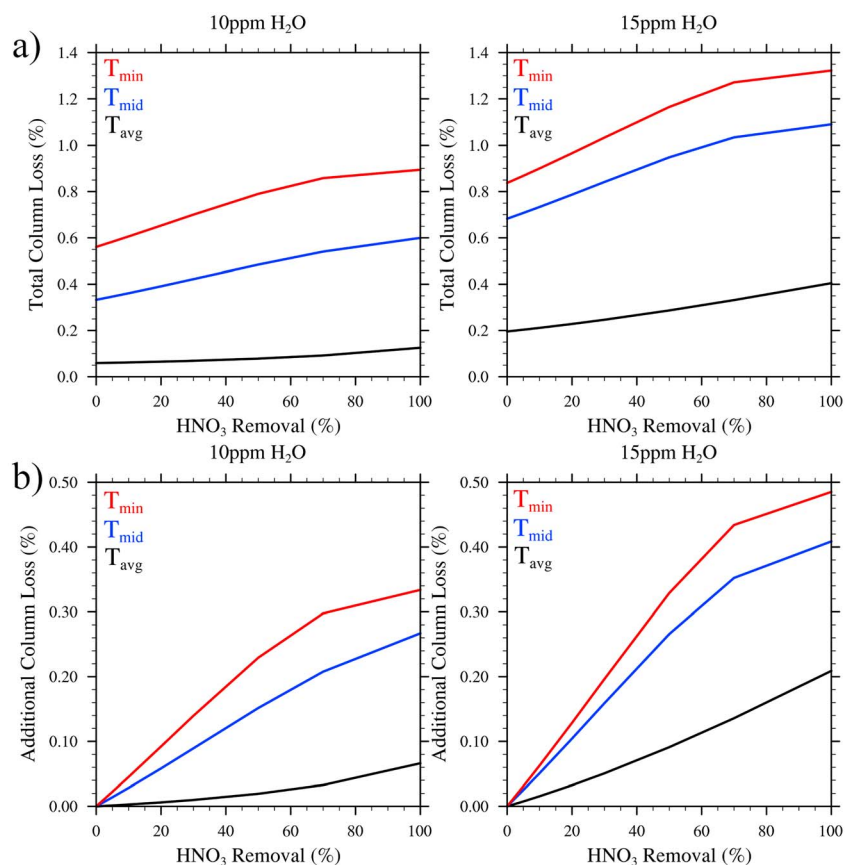


**Figure 12.** (a) Column ozone loss after 7 days of simulated elevated water vapor as a function of initial HNO<sub>3</sub> percent removal at 10 and 15 ppmv of water vapor for  $T_{avg}$ ,  $T_{mid}$ , and  $T_{min}$  as indicated by color. (b) The increase in column ozone loss due to initial nitric acid removal above the corresponding control simulation as a function of initial HNO<sub>3</sub> percent removal for the simulations shown in (a).

Similarly, the sensitivity of each simulation to the amount of initial HNO<sub>3</sub> removed at different altitudes within the lower stratosphere also depends on the favorability of the initial conditions at that altitude to the chlorine activation chemical mechanism. Figure 11 summarizes the dependence of additional chlorine activation resulting from HNO<sub>3</sub> removal after 36 hr on the magnitude of initial HNO<sub>3</sub> removal at each potential temperature level for 10 and 15 ppmv of water vapor at  $T_{avg}$ ,  $T_{mid}$ , and  $T_{min}$ . The simulations with colder temperature profiles and higher initial water vapor concentrations generally showed higher sensitivity to HNO<sub>3</sub> removal at both low and high magnitudes of removal. Simulations unfavorable to chlorine activation, such as 10 ppmv of water vapor at  $T_{avg}$ , were insensitive to even large amounts of HNO<sub>3</sub> removal up to 100% removal. Within the vertical structure of the lower stratosphere, sensitivity to the magnitude of initial HNO<sub>3</sub> removal was influenced by the altitude dependence of temperature and background inorganic chlorine. Again, the coldest levels (370–390 K) showed the greatest response to HNO<sub>3</sub> removal across all initial temperature and water vapor conditions. In the simulations most favorable to chlorine activation, including 10 ppmv of water vapor at  $T_{min}$  and 15 ppmv of water vapor at both  $T_{mid}$  and  $T_{min}$ , the increasing concentration of background inorganic chlorine at upper levels began to influence the sensitivity to HNO<sub>3</sub> removal. Under these conditions, 400 and 410 K began to exhibit significant increases in reactive chlorine concentrations due to HNO<sub>3</sub> removal even greater than increases at the coldest levels in the most extreme initial conditions. Finally, Figure 11 also shows a “saturation point” beyond which increases in HNO<sub>3</sub> removal result in much lower additional reactive chlorine concentrations at certain levels (e.g., 380 and 390 K at  $T_{mid}$  and  $T_{min}$  with 15 ppmv of water vapor). This “saturation” of the HNO<sub>3</sub> removal effect at approximately 70% removal occurs under the conditions most favorable to chlorine activation, that is, the coldest and most humid simulations.

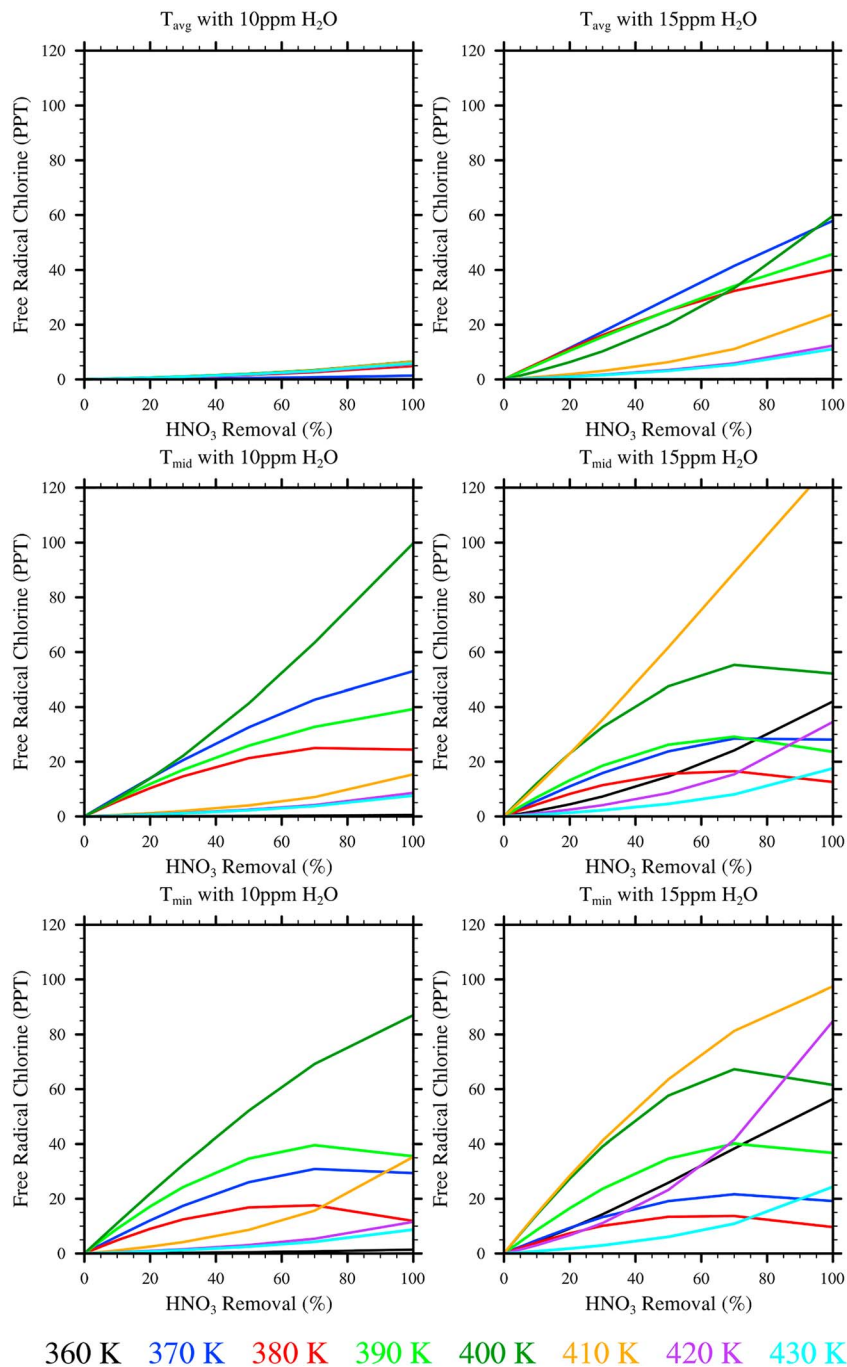


**Figure 13.** As in Figure 11 but for  $6\text{-}\mu\text{m}^2/\text{cm}^3$  sulfate aerosol surface area density. PPT = parts per trillion.

At 70% initial  $\text{HNO}_3$  removal, the reduction of the  $\text{NO}_x$  source has resulted in an almost complete removal of  $\text{NO}_x$  at the steady state achieved by 36 hr. Therefore, additional removal of initial  $\text{HNO}_3$  cannot further influence the chlorine activation chemical mechanism under these conditions.

Figure 12a shows the column ozone loss resulting from chlorine activation after 7 days of elevated water vapor concentration due to initial  $\text{HNO}_3$  removal for simulations with 10 and 15 ppmv of initial water vapor at  $T_{\text{avg}}$ ,  $T_{\text{mid}}$ , and  $T_{\text{min}}$  as a function of the magnitude of  $\text{HNO}_3$  removal. Figure 12b shows the additional column ozone loss resulting from initial  $\text{HNO}_3$  removal as a function of  $\text{HNO}_3$  removal magnitude.

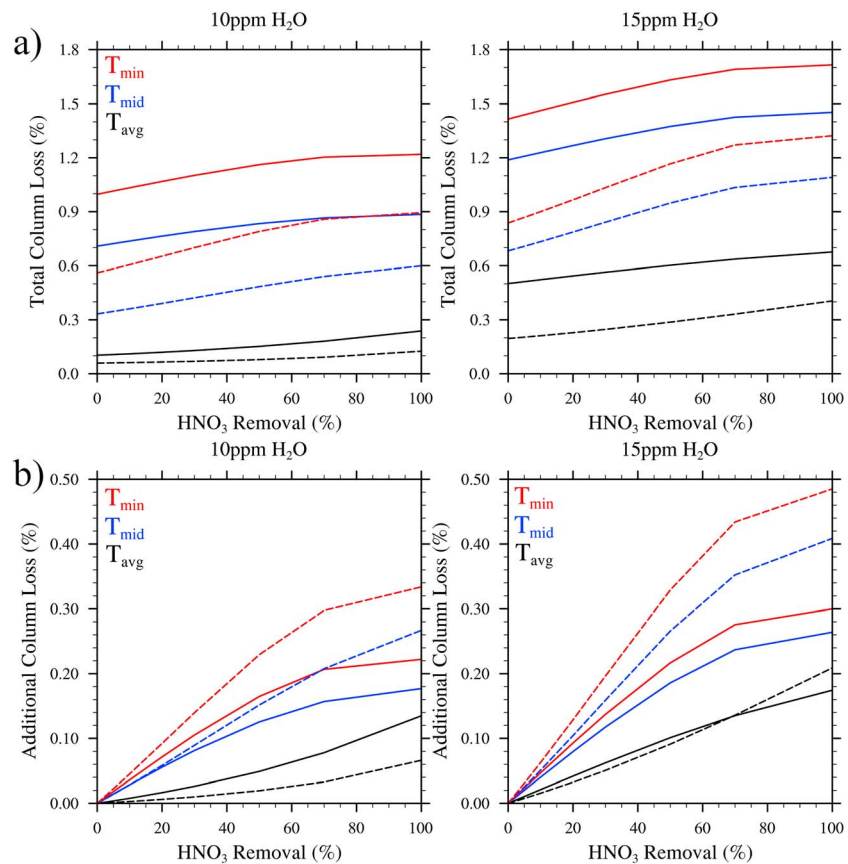


**Figure 14.** As in Figure 12 but for 6- $\mu\text{m}^2/\text{cm}^3$  sulfate aerosol surface area density, with results for the corresponding simulations with 2- $\mu\text{m}^2/\text{cm}^3$  sulfate aerosol surface area density shown by the dashed lines.

Column ozone loss was calculated using NASA's Earth Observing System-Aura Ozone Monitoring Instrument data set (Levelt et al., 2006) over the region of interest. The total ozone loss value was taken as the sum of ozone loss over all simulated potential temperature levels (360–430 K) and the initial ozone column value was taken from the Ozone Monitoring Instrument measurement. Because column ozone loss is directly dependent on the concentration of free radical chlorine, the effect of initial HNO<sub>3</sub> removal magnitude on column ozone loss follows the trends of chlorine activation discussed above. The magnitude of additional column ozone loss due to HNO<sub>3</sub> removal increased under colder and more humid conditions because the effect of decreasing a NO<sub>x</sub> source through HNO<sub>3</sub> removal on the chlorine activation chemical mechanism depends on preexisting chlorine activation independent of the HNO<sub>3</sub> removal. This increase in sensitivity to the magnitude of initial HNO<sub>3</sub> removal due to the favorability of initial temperature and water vapor conditions to chlorine activation also reaches a saturation point at approximately 70% removal under the coldest and most humid conditions (e.g., 10 ppmv of water vapor at  $T_{\text{min}}$  and 15 ppmv of water vapor at  $T_{\text{mid}}$  and  $T_{\text{min}}$ ). Beyond this point additional HNO<sub>3</sub> removal results in no further reduction in the steady state concentration of NO<sub>x</sub> and therefore no further increase in free radical chlorine concentration and ozone loss.

### 3.3. Elevated Sulfate Aerosol SAD Simulations

Because of the dependence of the effect of HNO<sub>3</sub> removal on the favorability of initial conditions to the chlorine activation chemical mechanism and the resulting free radical chlorine concentration, the effect of HNO<sub>3</sub> removal under conditions of higher sulfate aerosol SAD is a result of the impact of higher SAD on the amount of chlorine activation. In general, higher sulfate aerosol SAD leads to more chlorine activation and subsequent ozone loss because of the linear dependence of the chlorine activation heterogeneous reaction rates, which drive the chemical mechanism, on SAD. As a result, the initial temperature and

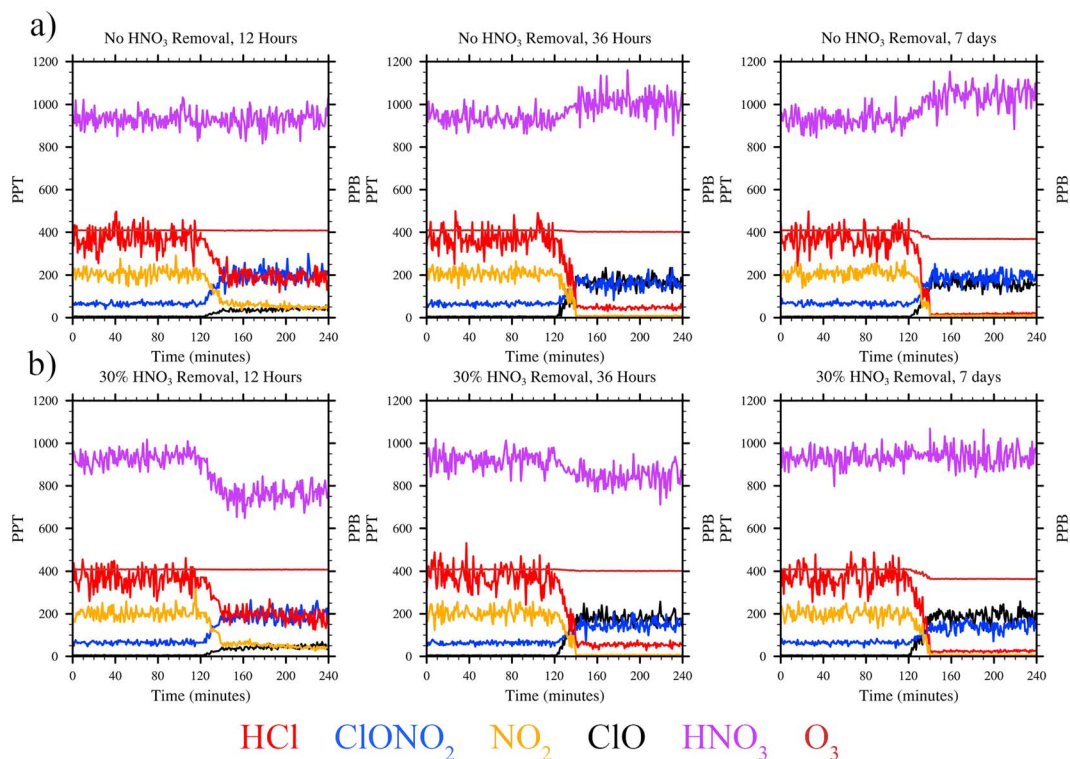


**Figure 15.** Hypothetical observations of HCl, ClONO<sub>2</sub>, ClO, NO<sub>2</sub>, and O<sub>3</sub> across the transition between background stratospheric air and a convectively influenced air mass of 10-ppmv elevated water vapor at 103.6 hPa and 198.8 K 12 hr, 36 hr, and 7 days after injection with (a) no nitric acid removal and (b) 30% nitric acid removal. The unperturbed background stratospheric measurements would occur between 0 and 120 min, and the convectively perturbed measurements would occur from 120 until 240 min. Ozone is shown in units of parts per billion (PPB) by volume (right axis) and all other species are in units of parts per trillion (PPT) by volume (left axis).

water vapor conditions of all simulations become more favorable to the chlorine activation chemical mechanism. This increase in baseline chlorine activation changes both which initial conditions and what vertical range within the lower stratosphere within a given set of initial conditions are sensitive to the effects of HNO<sub>3</sub> removal.

Figure 13a shows the effects of initial HNO<sub>3</sub> removal on reactive chlorine concentrations after 36 hr over the lower stratosphere profile for 10 and 15 ppmv at  $T_{avg}$ ,  $T_{mid}$ , and  $T_{min}$  with an elevated sulfate aerosol SAD of 6  $\mu\text{m}^2/\text{cm}^3$ . Figure 13b shows the anomalies of the additional reactive chlorine concentrations resulting from HNO<sub>3</sub> removal when comparing the 6- $\mu\text{m}^2/\text{cm}^3$  SAD to 2- $\mu\text{m}^2/\text{cm}^3$  SAD simulations. With an increase in baseline chlorine activation resulting from the additional sulfate aerosol, simulations with initial conditions previously too warm and/or not sufficiently humid to be sensitive to the effects of HNO<sub>3</sub> removal showed increasing reactive chlorine concentrations resulting from HNO<sub>3</sub> removal. For example, while at 2- $\mu\text{m}^2/\text{cm}^3$  360 and 420 K only show a sensitivity to HNO<sub>3</sub> removal at extreme case of 15 ppmv of water vapor and  $T_{min}$ , at 6- $\mu\text{m}^2/\text{cm}^3$  SAD they show sensitivity to HNO<sub>3</sub> removal also at 15 ppmv of water vapor and  $T_{mid}$ , and an increased response at  $T_{min}$ . Similarly, more altitudes under initial conditions that are sensitive to HNO<sub>3</sub> removal display the “saturation” effect beyond which additional HNO<sub>3</sub> removal does not result in significantly more reactive chlorine at 6- $\mu\text{m}^2/\text{cm}^3$  SAD that had not previously at 2- $\mu\text{m}^2/\text{cm}^3$  SAD (e.g., 400 K at 15 ppmv of water vapor at  $T_{mid}$ ). Further, at these levels, although HNO<sub>3</sub> removal still increases the concentration of reactive chlorine, the effect is smaller in magnitude at 6- $\mu\text{m}^2/\text{cm}^3$  SAD. The reason is that as the chlorine activation reactions become more favored and a greater fraction of reservoir inorganic chlorine is converted to reactive chlorine, the effect of removing a NO<sub>x</sub> source on increasing reactive chlorine concentrations becomes comparatively less significant.

The overall effect is that, although higher sulfate aerosol SAD resulted in more total column ozone loss, the same amount of initial  $\text{HNO}_3$  removal resulted in a smaller increase in column ozone loss at  $6\text{-}\mu\text{m}^2/\text{cm}^3$  SAD than at  $2\text{-}\mu\text{m}^2/\text{cm}^3$  SAD for most initial conditions. Figure 14a shows the total column ozone loss after 7 days of elevated water vapor at  $6\text{-}\mu\text{m}^2/\text{cm}^3$  SAD (solid lines) and  $2\text{-}\mu\text{m}^2/\text{cm}^3$  SAD (dashed lines) as a function of percent  $\text{HNO}_3$  removal for 10- and 15-ppmv water vapor and  $T_{\text{avg}}$ ,  $T_{\text{mid}}$ , and  $T_{\text{min}}$ . Figure 14b shows the additional column ozone loss resulting from initial  $\text{HNO}_3$  removal for the same simulations. Only at 10 ppmv of water vapor at  $T_{\text{avg}}$  did  $\text{HNO}_3$  have a significantly greater impact on column ozone loss at  $6\text{-}\mu\text{m}^2/\text{cm}^3$  SAD compared to  $2\text{-}\mu\text{m}^2/\text{cm}^3$  SAD. This is because in most simulations, the “saturation” effect of the greater favorability of the chlorine activation chemical mechanism outweighed the additional sensitivity to  $\text{HNO}_3$  removal at the higher temperatures of the upper altitudes that most contributed to increases in ozone loss.

#### 4. Conclusions

In summary, stratospheric  $\text{HNO}_3$  removal by convectively lofted ice that sediments out of the stratosphere rather than sublimates has the greatest effect of increasing chlorine activation and ozone loss under initial temperature and humidity conditions that favor chlorine activation but have not yet maximized the heterogeneous reaction rates. This is because  $\text{HNO}_3$  removal interacts with the chlorine activation chemical mechanism by decreasing potential  $\text{NO}_x$  sources in the lower stratosphere, thereby allowing for greater concentrations of reactive chlorine after 36 hr of elevated water vapor. Increasing the amount of  $\text{HNO}_3$  removed increases the resulting additional free radical chlorine and subsequent ozone loss from the chlorine activation chemical mechanism. This effect can “saturate,” however, once  $\text{NO}_x$  concentrations at 36 hr are reduced to approximately 0, beyond which further  $\text{HNO}_3$  removal has no effect (occurring at approximately 70%  $\text{HNO}_3$  removal). With conditions that allow for little or no chlorine activation,  $\text{HNO}_3$  removal has no significant effect because the loss of potential  $\text{NO}_x$  sources has no impact if no free radical chlorine is present.  $\text{HNO}_3$  removal, therefore, has the greatest potential to increase chlorine activation and ozone loss in the regime of conditions that weakly favor the chlorine activation chemical mechanism in which the removal of a  $\text{NO}_x$  source has the largest impact on the total concentration of activated free radical chlorine.

Under conditions of elevated sulfate aerosol SAD resulting from a potential future volcanic eruption or SRM, the lower stratosphere is more sensitive to convectively elevated water vapor concentrations: The same amount of elevated initial water vapor led to greater chlorine activation and ozone loss. The effects of potential  $\text{HNO}_3$  removal by convection, however, were lesser in magnitude because of the overall increase in favorability to the chlorine activation chemical mechanism resulting from greater sulfate aerosol SAD. The simulated initial temperature and humidity conditions independent of  $\text{HNO}_3$  removal more readily reached almost complete  $\text{NO}_x$  removal. As a result, reducing a  $\text{NO}_x$  source by removing initial  $\text{HNO}_3$  had less of an effect on the increase in free radical chlorine concentrations than under background sulfate aerosol SAD conditions.

Compared to previous modeling of the effect of convectively injected water vapor enhancements on the chemistry of the lower stratosphere (Anderson et al., 2012; Anderson et al., 2017; Anderson & Clapp, 2018), this study investigates the range of chemical response to potential convective  $\text{HNO}_3$  removal concurrent with water vapor enhancements. We show that the chemical impact of small convective water vapor enhancements on reactive chlorine concentrations is highly sensitive to  $\text{HNO}_3$  removal, particularly at colder temperatures where even 5% removal resulted in additional ozone loss. Limitations of the model, however, restrict the conclusions that can be drawn from these results. To begin with, the model only simulates the chemistry within a convectively influenced air mass and does not allow for mixing with the surrounding stratosphere. As a result, the extent of chlorine activation and ozone loss represent an upper limit for that convectively influenced air mass. The model also does not account for radiative cooling or temperature fluctuations due to gravity waves. These effects could exacerbate the effects of convectively enhanced water vapor due to the sensitivity of the chlorine activation chemical mechanism to temperature. Finally, the chlorine activation and column ozone loss reported only affects the convectively perturbed stratospheric volume, not the stratosphere as a whole, and the area beneath the convectively influenced air mass.

Therefore, to better assess the large-scale significance of the chemical impact convectively enhanced water vapor on the lower stratosphere, an observational climatology of the parameters of convective injection including potential  $\text{HNO}_3$  removal (as implied by this work), water vapor mass transported, enhancement lifetime and mixing rates, and geographic coverage and of lower stratospheric temperatures are necessary. Observations that allowed for an estimated conversion between radar observations of only condensed phase volumes, to total water vapor transported would dramatically increase our ability to assess the extent of convective perturbations to the lower stratosphere. Complementary measurements of key chemical species in the chlorine activation chemical mechanism made in convective outflow would verify and constrain the calculations of potential chlorine activation and ozone loss. Figure 15 illustrates a hypothetical observation of the boundary between the background stratosphere and a convectively influenced air mass with the concentrations of chemical species relevant to the chlorine activation chemical mechanism as a function of time at various points in the lifetime of the air mass based on the model results. Measurements of (a)  $\text{NO}_2$  would allow for tracking of the first phase of chlorine activation, of (b)  $\text{HCl}$  and  $\text{ClONO}_2$  would allow for tracking both the repartitioning in the first phase and the activation of inorganic chlorine in the second phase, of (c)  $\text{ClO}$  would allow for tracking the net result of chlorine activation, (d)  $\text{HNO}_3$  would allow for observing any convective  $\text{HNO}_3$  removal, and of (e)  $\text{O}_3$  would allow for tracking of the potential subsequent catalytic loss rate of ozone in the presence of  $\text{ClO}$  and  $\text{BrO}$ . Observations of the stratospheric chemical composition over time across the boundary between the background stratosphere and the convective plume would show the effect of mixing on the chlorine activation chemical mechanism. A long-term record of such observations would also allow for a better evaluation of the large-scale chemical significance of convective injection by resolving the likelihood of the physical and chemical parameters of convectively influenced air masses necessary to result in chlorine activation and ozone loss.

#### Acknowledgments

There are no conflicts of interest to declare. Data from the SEAC<sup>4</sup>RS mission can be downloaded at <https://www-air.larc.nasa.gov/missions/seac4rs/dataaccess.htm>. The original NEXRAD data are available at the NOAA National Centers for Environmental Information site at <https://www.ncdc.noaa.gov/data-access-radar-data/nexrad>. MLS data are available for download at <https://mirador.gsfc.nasa.gov>. We would like to thank the members of the Anderson group for their support and to thank Jack Cooney for sharing his ongoing analysis and processing of the 10-year NEXRAD climatology. This work has been supported by the National Aeronautics and Space Administration (NASA) under NASA award NNX15AF60G (UV Absorption Cross Sections and Equilibrium Constant of  $\text{ClOOC}$  Determined from New Laboratory Spectroscopy Studies of  $\text{ClOOC}$  and  $\text{ClO}$ ) and a grant from the National Science Foundation (NSF) Arctic Observing Network (AON) Program under NSF award 1203583 (Collaborative Research: Multi-Regional Scale Aircraft Observations of Methane and Carbon Dioxide Isotopic Fluxes in the Arctic).

#### References

- Abbatt, J. P. D. (1997). Interaction of  $\text{HNO}_3$  with water-ice surfaces at temperatures of the free troposphere. *Geophysical Research Letters*, 24(12), 1479–1482. <https://doi.org/10.1029/97GL01403>
- Abbatt, J. P. D. (2003). Interactions of atmospheric trace gases with ice surfaces: Adsorption and reaction. *Chemical Reviews*, 103(12), 4783–4800. <https://doi.org/10.1021/cr0206418>
- Aguzzi, A., & Rossi, M. J. (2001). The kinetics of the uptake of  $\text{HNO}_3$  on ice, solid  $\text{H}_2\text{SO}_4\text{-H}_2\text{O}$  and solid ternary solutions of  $\text{H}_2\text{SO}_4\text{-HNO}_3\text{-H}_2\text{O}$  in the temperature range 180–211 K. *Physical Chemistry Chemical Physics*, 3(17), 3707–3716. <https://doi.org/10.1039/b100546g>
- Anderson, J. G., & Clapp, C. E. (2018). Coupling free radical catalysis, climate change, and human health. *Physical Chemistry Chemical Physics*, 20(16), 10,569–10,587. <https://doi.org/10.1039/C7CP08331A>
- Anderson, J. G., Weisenstein, D. K., Bowman, K. P., Homeyer, C. R., Smith, J. B., Wilmouth, D. M., et al. (2017). Stratospheric ozone over the United States in summer linked to observations of convection and temperature via chlorine and bromine catalysis. *Proceedings of the National Academy of Sciences*, 114(25), E4905–E4913. <https://doi.org/10.1073/pnas.1619318114>
- Anderson, J. G., Wilmouth, D. M., Smith, J. B., & Sayres, D. S. (2012). UV dosage levels in summer: Increased risk of ozone loss from convectively injected water vapor. *Science*, 337(6096), 835–839. <https://doi.org/10.1126/science.1222978>
- Aschmann, J., Sinnhuber, B.-M., Atlas, E. L., & Schauffler, S. M. (2009). Modeling the transport of very short-lived substances into the tropical upper troposphere and lower stratosphere. *Atmospheric Chemistry and Physics*, 9(23), 9237–9247. <https://doi.org/10.5194/acp-9-9237-2009>
- Audiffren, N., Cautenet, S., & Chaumerliac, N. (1999). A modeling study of the influence of ice scavenging on the chemical composition of liquid-phase precipitation of a cumulonimbus cloud. *Journal of Applied Meteorology*, 38(8), 1148–1160. [https://doi.org/10.1175/1520-0450\(1999\)038<1148:AMSOTI>2.0.CO;2](https://doi.org/10.1175/1520-0450(1999)038<1148:AMSOTI>2.0.CO;2)
- Austin, J., Scinocca, J., Plummer, D., Oman, L., Waugh, D., Akiyoshi, H., et al. (2010). Decline and recovery of total column ozone using a multimodel time series analysis. *Journal of Geophysical Research*, 115, D00M10. <https://doi.org/10.1029/2010JD013857>
- Avallone, L. M., Toohey, D. W., Proffitt, M. H., Margitan, J. J., Chan, K. R., & Anderson, J. G. (1993). In situ measurements of  $\text{ClO}$  at mid-latitudes: Is there an effect from Mt. Pinatubo? *Geophysical Research Letters*, 20(22), 2519–2522. <https://doi.org/10.1029/93GL02418>
- Ball, W. T., Alsing, J., Mortlock, D. J., Staehelin, J., Haigh, J. D., Peter, T., et al. (2018). Evidence for a continuous decline in lower stratospheric ozone offsetting ozone layer recovery. *Atmospheric Chemistry and Physics*, 18(2), 1379–1394. <https://doi.org/10.5194/acp-18-1379-2018>
- Barth, M. C., Stuart, A. L., & Skamarock, W. C. (2001). Numerical simulations of the July 10, 1996, stratospheric-tropospheric experiment: Radiation, Aerosols, and Ozone (STERAO)-deep convection experiment storm: Redistribution of soluble tracers. *Journal of Geophysical Research*, 106(D12), 12,381–12,400. <https://doi.org/10.1029/2001JD900139>
- Borrmann, S., Solomon, S., Avallone, L., Toohey, D., & Baumgardner, D. (1997). On the occurrence of  $\text{ClO}$  in cirrus clouds and volcanic aerosol in the tropopause region. *Geophysical Research Letters*, 24(16), 2011–2014. <https://doi.org/10.1029/97GL02053>
- Borrmann, S., Solomon, S., Dye, J. E., & Luo, B. (1996). The potential of cirrus clouds for heterogeneous chlorine activation. *Geophysical Research Letters*, 23(16), 2133–2136. <https://doi.org/10.1029/96GL01957>
- Brune, W. H., Toohey, D. W., Anderson, J. G., & Chan, K. R. (1990). In situ observations of  $\text{ClO}$  in the Arctic stratosphere: ER-2 aircraft results from 59°N to 80°N latitude. *Geophysical Research Letters*, 17(4), 505–508. <https://doi.org/10.1029/GL017i004p00505>
- Butchart, N. (2014). The Brewer-Dobson circulation. *Reviews of Geophysics*, 52, 157–184. <https://doi.org/10.1002/2013RG000448>
- Carslaw, K. S., Peter, T., & Clegg, S. L. (1997). Modeling the composition of liquid stratospheric aerosols. *Reviews of Geophysics*, 35(2), 125–154. <https://doi.org/10.1029/97rg00078>

- Chipperfield, M. P., Bekki, S., Dhomse, S., Harris, N. R. P., Hassler, B., Hossaini, R., et al. (2017). Detecting recovery of the stratospheric ozone layer. *Nature*, *549*(7671), 211–218. <https://doi.org/10.1038/nature23681>
- Chipperfield, M. P., Dhomse, S., Hossaini, R., Feng, W., Santee, M. L., Weber, M., et al. (2018). On the cause of recent variations in lower stratospheric ozone. *Geophysical Research Letters*, *45*(11), 5718–5726. <https://doi.org/10.1029/2018GL078071>
- Chipperfield, M. P., & Pyle, J. A. (1998). Model sensitivity studies of Arctic ozone depletion. *Journal of Geophysical Research*, *103*(D21), 29,389–28,493. <https://doi.org/10.1029/98jd01960>
- Cooney, J. W., Bowman, K. P., Homeyer, C. R., & Fenske, T. M. (2018). Ten year analysis of tropopause-overshooting convection using GridRad data. *Journal of Geophysical Research: Atmospheres*, *123*, 329–343. <https://doi.org/10.1002/2017JD027718>
- Corti, T., Luo, B. P., de Reus, M., Brunner, D., Cairo, F., Mahoney, M. J., et al. (2008). Unprecedented evidence for deep convection hydrating the tropical stratosphere. *Geophysical Research Letters*, *35*, L10810. <https://doi.org/10.1029/2008GL033641>
- Dauhut, T., Chaboureaud, J.-P., Haynes, P. H., & Lane, T. P. (2018). The mechanisms leading to a stratospheric hydration by overshooting convection. *Journal of the Atmospheric Sciences*, *75*(12), 4383–4398. <https://doi.org/10.1175/JAS-D-18-0176.1>
- de Reus, M., Borrmann, S., Bansemer, A., Heymsfield, A. J., Weigel, R., Schiller, C., et al. (2009). Evidence for ice particles in the tropical stratosphere from in-situ measurements. *Atmospheric Chemistry and Physics*, *9*(18), 6775–6792. <https://doi.org/10.5194/acp-9-6775-2009>
- Dessens, O., Zeng, G., Warwick, N., & Pyle, J. (2009). Short-lived bromine compounds in the lower stratosphere; impact of climate change on ozone. *Atmospheric Science Letters*, *10*(3), 201–206. <https://doi.org/10.1002/asl.236>
- Dessler, A. E., Hanco, T. F., & Fueglistaler, S. (2007). Effects of convective ice lofting on H<sub>2</sub>O and HDO in the tropical tropopause layer. *Journal of Geophysical Research*, *112*(D18), D18309. <https://doi.org/10.1029/2007JD008609>
- Dessler, A. E., & Sherwood, S. C. (2004). Effect of convection on the summertime extratropical lower stratosphere. *Journal of Geophysical Research*, *109*(D23), D23301. <https://doi.org/10.1029/2004JD005209>
- Diffenbaugh, N. S., Scherer, M., & Trapp, R. J. (2013). Robust increases in severe thunderstorm environments in response to greenhouse forcing. *Proceedings of the National Academy of Sciences*, *110*(41), 16,361–16,366. <https://doi.org/10.1073/pnas.1307758110>
- Drdla, K., & Müller, R. (2012). Temperature thresholds for chlorine activation and ozone loss in the polar stratosphere. *Annales Geophysicae*, *30*(7), 1055–1073. <https://doi.org/10.5194/angeo-30-1055-2012>
- Dykema, J. A., Keith, D. W., Anderson, J. G., & Weisenstein, D. (2014). Stratospheric controlled perturbation experiment: A small-scale experiment to improve understanding of the risks of solar geoengineering. *Philosophical Transactions of the Royal Society A*, *372*, 20140059. <https://doi.org/10.1098/rsta.2014.0059>
- Engel, A., Bönisch, H., Ostermüller, J., Chipperfield, M. P., Dhomse, S., & Jöckel, P. (2018). A refined method for calculating equivalent effective stratospheric chlorine. *Atmospheric Chemistry and Physics*, *18*(2), 601–619. <https://doi.org/10.5194/acp-18-601-2018>
- Fahey, D. W., Eubank, C. S., Hübler, G., & Fehsenfeld, F. C. (1985). Evaluation of a catalytic reduction technique for the measurement of total reactive odd-nitrogen NO<sub>y</sub> in the atmosphere. *Journal of Atmospheric Chemistry*, *3*(4), 435–468. <https://doi.org/10.1007/BF00053871>
- Fahey, D. W., Kawa, S. R., Woodbridge, E. L., Tin, P., Wilson, J. C., Jonsson, H. H., et al. (1993). In situ measurements constraining the role of sulphate aerosols in mid-latitude ozone depletion. *Nature*, *363*(6429), 509–514. <https://doi.org/10.1038/363509a0>
- Falk, S., Sinnhuber, B.-M., Krysztofiak, G., Jöckel, P., Graf, P., & Lennartz, S. T. (2017). Brominated VLS and their influence on ozone under a changing climate. *Atmospheric Chemistry and Physics*, *17*(18), 11,313–11,329. <https://doi.org/10.5194/acp-17-11313-2017>
- Feng, Z., Leung, R., Hagos, S., Houze, R. A., Burleyson, C. D., & Balaguru, K. (2016). More frequent intense and long-lived storms dominate the springtime trend in central US rainfall. *Nature Communications*, *7*, 13429. <https://doi.org/10.1038/ncomms13429>
- Fernandez, R. P., Kinnison, D. E., Lamarque, J.-F., Tilmes, S., & Saiz-Lopez, A. (2017). Impact of biogenic very short-lived bromine on the Antarctic ozone hole during the 21st century. *Atmospheric Chemistry and Physics*, *17*(3), 1673–1688. <https://doi.org/10.5194/acp-17-1673-2017>
- Frey, W., Schofield, R., Hoor, P., Kunkel, D., Ravegnani, F., Ulanovsky, A., et al. (2015). The impact of overshooting deep convection on local transport and mixing in the tropical upper troposphere/lower stratosphere (UTLS). *Atmospheric Chemistry and Physics*, *15*(11), 6467–6486. <https://doi.org/10.5194/acp-15-6467-2015>
- Fueglistaler, S., Bonazzola, M., Haynes, P. H., & Peter, T. (2005). Stratospheric water vapor predicted from the Lagrangian temperature history of air entering the stratosphere in the tropics. *Journal of Geophysical Research*, *110*, D08107. <https://doi.org/10.1029/2004JD005516>
- Gamblin, B., Toon, O. B., Tolbert, M. A., Kondo, Y., Takegawa, N., Irie, H., et al. (2007). Nitric acid condensation on ice: 2. Kinetic limitations, a possible “cloud clock” for determining cloud parcel lifetime. *Journal of Geophysical Research*, *112*, D12209. <https://doi.org/10.1029/2005JD006049>
- Grosvenor, D. P., Choulaton, T. W., Coe, H., & Held, G. (2007). A study of the effect of overshooting deep convection on the water content of the TTL and lower stratosphere from cloud resolving model simulations. *Atmospheric Chemistry and Physics*, *7*(18), 4977–5002. <https://doi.org/10.5194/acp-7-4977-2007>
- Hanisco, T. F., Moyer, E. J., Weinstock, E. M., St. Clair, J. M., Sayres, D. S., Smith, J. B., et al. (2007). Observations of deep convective influence on stratospheric water vapor and its isotopic composition. *Geophysical Research Letters*, *34*, L04814. <https://doi.org/10.1029/2006GL027899>
- Hanson, D. R. (1998). Reaction of ClONO<sub>2</sub> with H<sub>2</sub>O and HCl in sulfuric acid and HNO<sub>3</sub>/H<sub>2</sub>SO<sub>4</sub>/H<sub>2</sub>O mixtures. *Journal of Physical Chemistry A*, *102*(25), 4794–4807. <https://doi.org/10.1021/jp972767s>
- Hassim, M. E. E., & Lane, T. P. (2010). A model study on the influence of overshooting convection on TTL water vapour. *Atmospheric Chemistry and Physics*, *10*(20), 9833–9849. <https://doi.org/10.5194/acp-10-9833-2010>
- Hegglin, M. I., Brunner, D., Wernli, H., Schwierz, C., Martius, O., Hoor, P., et al. (2004). Tracing troposphere-to-stratosphere transport above a mid-latitude deep convective system. *Atmospheric Chemistry and Physics*, *4*(3), 741–756. <https://doi.org/10.5194/acp-4-741-2004>
- Hofmann, D. J., Oltmans, S. J., Komhyr, W. D., Harris, J. M., Lathrop, J. A., Langford, A. O., et al. (1994). Ozone loss in the lower stratosphere over the United States in 1992–1993: Evidence for heterogeneous chemistry on the Pinatubo aerosol. *Geophysical Research Letters*, *21*(1), 65–68. <https://doi.org/10.1029/93GL02526>
- Hofmann, D. J., & Solomon, S. (1989). Ozone destruction through heterogeneous chemistry following the eruption of El Chichón. *Journal of Geophysical Research*, *94*(D4), 5029–5041. <https://doi.org/10.1029/JD094iD04p05029>
- Holton, J. R., Haynes, P. H., McIntyre, M. E., Douglass, A. R., Rood, R. B., & Pfister, L. (1995). Stratosphere-troposphere exchange. *Reviews of Geophysics*, *33*(4), 403–439. <https://doi.org/10.1029/95RG02097>
- Homeyer, C. R. (2014). Formation of the enhanced-V infrared cloud-top feature from high-resolution three-dimensional radar observations. *Journal of the Atmospheric Sciences*, *71*(1), 332–348. <https://doi.org/10.1175/JAS-D-13-079.1>

- Homeyer, C. R., McAuliffe, J. D., & Bedka, K. M. (2017). On the development of above-anvil cirrus plumes in extratropical convection. *Journal of the Atmospheric Sciences*, *74*(5), 1617–1633. <https://doi.org/10.1175/JAS-D-16-0269.1>
- Horn, A. B., Sodeau, J. R., Roddis, T. B., & Williams, N. A. (1998). Mechanism of the heterogeneous reaction of hydrogen chloride with chlorine nitrate and hypochlorous acid on water ice. *Journal of Physical Chemistry A*, *102*(30), 6107–6120. <https://doi.org/10.1021/jp973083n>
- Hossaini, R., Chipperfield, M. P., Dhomse, S., Ordóñez, C., Saiz-Lopez, A., Abraham, N. L., et al. (2012). Modelling future changes to the stratospheric source gas injection of biogenic bromocarbons. *Geophysical Research Letters*, *39*, L20813. <https://doi.org/10.1029/2012GL053401>
- Hossaini, R., Chipperfield, M. P., Montzka, S. A., Leeson, A. A., Dhomse, S. S., & Pyle, J. A. (2017). The increasing threat to stratospheric ozone from dichloromethane. *Nature Communications*, *8*, 15962. <https://doi.org/10.1038/ncomms15962>
- Hossaini, R., Chipperfield, M. P., Montzka, S. A., Rap, A., Dhomse, S., & Feng, W. (2015). Efficiency of short-lived halogens at influencing climate through depletion of stratospheric ozone. *Nature Geoscience*, *8*(3), 186–190. <https://doi.org/10.1038/ngeo2363>
- Hossaini, R., Chipperfield, M. P., Saiz-Lopez, A., Harrison, J. J., von Glasow, R., Sommariva, R., et al. (2015). Growth in stratospheric chlorine from short-lived chemicals not controlled by the Montreal Protocol. *Geophysical Research Letters*, *42*, 4573–4580. <https://doi.org/10.1002/2015GL064783>
- Hossaini, R., Patra, P. K., Leeson, A. A., Krysztofciak, G., Abraham, N. L., Andrews, S. J., et al. (2016). A multi-model intercomparison of halogenated very short-lived substances (TransCom-VLSL): Linking oceanic emissions and tropospheric transport for a reconciled estimate of the stratospheric source gas injection of bromine. *Atmospheric Chemistry and Physics*, *16*(14), 9163–9187. <https://doi.org/10.5194/acp-16-9163-2016>
- Huthwelker, T., Ammann, M., & Peter, T. (2006). The uptake of acidic gases on ice. *Chemical Reviews*, *106*(4), 1375–1444. <https://doi.org/10.1021/cr020506v>
- Hynes, R. G., Fernandez, M. A., & Cox, R. A. (2002). Uptake of HNO<sub>3</sub> on water-ice and coadsorption of HNO<sub>3</sub> and HCl in the temperature range 210–235 K. *Journal of Geophysical Research*, *107*(D24), 4797. <https://doi.org/10.1029/2001JD001557>
- Iwasaki, S., Shibata, T., Nakamoto, J., Okamoto, H., Ishimoto, H., & Kubota, H. (2010). Characteristics of deep convection measured by using the A-train constellation. *Journal of Geophysical Research*, *115*(D6), D06207. <https://doi.org/10.1029/2009JD013000>
- Iwasaki, S., Shibata, T., Okamoto, H., Ishimoto, H., & Kubota, H. (2012). Mixtures of stratospheric and overshooting air measured using A-Train sensors. *Journal of Geophysical Research*, *117*, D12207.
- Jensen, E., Ackerman, A. S., & Smith, J. A. (2007). Can overshooting convection dehydrate the tropical tropopause layer? *Journal of Geophysical Research*, *112*, D11209. <https://doi.org/10.1029/2006JD007943>
- Kawa, S. R., Newman, P. A., Lait, L. R., Schoeberl, M. R., Stimpfle, R. M., Kohn, D. W., et al. (1997). Activation of chlorine in sulfate aerosol as inferred from aircraft observations. *Journal of Geophysical Research*, *102*(D3), 3921–3933. <https://doi.org/10.1029/96JD01992>
- Keim, E. R., Fahey, D. W., Del Negro, L. A., Woodbridge, E. L., Gao, R. S., Wennberg, P. O., et al. (1996). Observations of large reductions in the NO/NO<sub>2</sub> near the mid-latitude tropopause and the role of heterogeneous chemistry. *Geophysical Research Letters*, *23*(22), 3223–3226. <https://doi.org/10.1029/96GL02593>
- Khaykin, S., Pommereau, J.-P., Korshunov, L., Yushkov, V., Nielsen, J., Larsen, N., et al. (2009). Hydration of the lower stratosphere by ice crystal geysers over land convective systems. *Atmospheric Chemistry and Physics*, *9*(6), 2275–2287. <https://doi.org/10.5194/acp-9-2275-2009>
- Khaykin, S., Pommereau, J.-P., Riviere, E. D., Held, G., Ploeger, F., Ghysels, M., et al. (2016). Evidence of horizontal and vertical transport of water in the Southern Hemisphere tropical tropopause layer (TTL) from high-resolution balloon observations. *Atmospheric Chemistry and Physics*, *16*(18), 12,273–12,286. <https://doi.org/10.5194/acp-16-12273-2016>
- Koby, T. R. (2016). Development of a trajectory model for the analysis of stratospheric water vapor, (Doctoral dissertation). Retrieved from Digital Access to Scholarship at Harvard (<http://nrs.harvard.edu/urn-3:HUL.InstRepos:33493564>). Cambridge, MA: Harvard University.
- Kondo, Y., Toon, O. B., Irie, H., Gamblin, B., Koike, M., Takegawa, N., et al. (2003). Uptake of reactive nitrogen on cirrus cloud particles in the upper troposphere and lowermost stratosphere. *Geophysical Research Letters*, *30*(4), 1154. <https://doi.org/10.1029/2002GL016539>
- Krämer, M., Schiller, C., Voigt, C., Schlager, H., & Popp, P. J. (2008). A climatological view of HNO<sub>3</sub> partitioning in cirrus clouds. *Quarterly Journal of the Royal Meteorological Society*, *134*(633), 905–912. <https://doi.org/10.1002/qj.253>
- Laube, J. C., Engel, A., Bönisch, H., Möbius, T., Worton, D. R., Sturges, W. T., et al. (2008). Contribution of very short-lived organic substances to stratospheric chlorine and bromine in the tropics—A case study. *Atmospheric Chemistry and Physics*, *8*(23), 7325–7334. <https://doi.org/10.5194/acp-8-7325-2008>
- Lawrence, M. G., & Crutzen, P. J. (1998). The impact of cloud particle gravitational settling on soluble trace gas distributions. *Tellus Series B: Chemical and Physical Meteorology*, *50*(3), 263–289. <https://doi.org/10.3402/tellusb.v50i3.16129>
- Levelt, P. F., van der Oord, G. H. J., Dobber, M. R., Malkki, A., Visser, H. J., de Vries, J., et al. (2006). The ozone monitoring instrument. *IEEE Transactions on Geoscience and Remote Sensing*, *44*(5), 1093–1101.
- Li, F., Stolarski, R. S., & Newman, P. A. (2009). Stratospheric ozone in the post-CFC era. *Atmospheric Chemistry and Physics*, *9*(6), 2207–2213. <https://doi.org/10.5194/acp-9-2207-2009>
- Liang, Q., Atlas, E., Blake, D., Dorf, M., Pfeilsticker, K., & Schaufli, S. (2014). Convective transport of very short lived bromocarbons to the stratosphere. *Atmospheric Chemistry and Physics*, *14*(11), 5781–5792. <https://doi.org/10.5194/acp-14-5781-2014>
- Maréchal, V., Pirre, M., Rivière, E. D., Povesle, N., Crowley, J. N., Freitas, S. R., & Longo, K. M. (2010). Modelling the reversible uptake of chemical species in the gas phase by ice particles formed in a convective cloud. *Atmospheric Chemistry and Physics*, *10*(10), 4977–5000. <https://doi.org/10.5194/acp-10-4977-2010>
- Mari, C., Jacob, D. J., & Bechtold, P. (2000). Transport and scavenging of soluble gases in a deep convective cloud. *Journal of Geophysical Research*, *105*(D17), 22,255–22,267. <https://doi.org/10.1029/2000JD900211>
- McElroy, M. B., Salawitch, R. J., Wofsy, S. C., & Logan, J. A. (1986). Reductions of Antarctic ozone due to synergistic interactions of chlorine and bromine. *Nature*, *321*(6072), 759–762. <https://doi.org/10.1038/321759a0>
- McGee, T. J., Newman, P., Gross, M., Singh, U., Godin, S., Lacoste, A.-M., & Megie, G. (1994). Correlation of ozone loss with the presence of volcanic aerosols. *Geophysical Research Letters*, *21*(25), 2801–2804. <https://doi.org/10.1029/94GL02350>
- Molina, L. T., & Molina, M. J. (1987). Production of Cl<sub>2</sub>O<sub>2</sub> from the self-reaction of the ClO radical. *Journal of Physical Chemistry*, *91*(2), 433–436. <https://doi.org/10.1021/j100286a035>
- Molina, M. J. (1989). Heterogeneous chemical processes in ozone depletion. In *Ozone Depletion, Greenhouse Gases, and Climate Change* (pp. 48–55). Washington, DC: National Research Council.

- Murphy, D. M., & Ravishankara, A. R. (1994). Temperature averages and rates of stratospheric reactions. *Geophysical Research Letters*, *21*(23), 2471–2474. <https://doi.org/10.1029/94GL02287>
- Neu, J. L., & Prather, M. J. (2012). Toward a more physical representation of precipitation scavenging in global chemistry models: Cloud overlap and ice physics and their impact on tropospheric ozone. *Atmospheric Chemistry and Physics*, *12*(7), 3289–3310. <https://doi.org/10.5194/acp-12-3289-2012>
- Oman, L. D., & Douglass, A. R. (2014). Improvements in total column ozone in GEOSCCM and comparisons with a new ozone-depleting substances scenario. *Journal of Geophysical Research: Atmospheres*, *119*, 5613–5624. <https://doi.org/10.1002/2014JD021590>
- Oram, D. E., Ashfold, M. J., Laube, J. C., Gooch, L. J., Humphrey, S., Sturges, W. T., et al. (2017). A growing threat to the ozone layer from short-lived anthropogenic chlorocarbons. *Atmospheric Chemistry and Physics*, *17*(19), 11,929–11,941. <https://doi.org/10.5194/acp-17-11929-2017>
- Phoenix, D. B., Homeyer, C. R., & Barth, M. C. (2017). Sensitivity of simulated convection-driven stratosphere-troposphere exchange in WRF-Chem to the choice of physical and chemical parameterization. *Earth and Space Science*, *4*, 454–471. <https://doi.org/10.1002/2017EA000287>
- Pitari, G., Aquila, V., Kravitz, B., Robock, A., Watanabe, S., Cionni, I., et al. (2014). Stratospheric ozone response to sulfate geoengineering: Results from the Geoengineering Model Intercomparison Project (GeoMIP). *Journal of Geophysical Research: Atmospheres*, *119*, 2629–2653. <https://doi.org/10.1002/2013JD020566>
- Pittman, J. V., Weinstock, E. M., Oglesby, R. J., Sayres, D. S., Smith, J. B., Anderson, J. G., et al. (2007). Transport in the subtropical lowermost stratosphere during the Cirrus Regional Study of Tropical Anvils and Cirrus Layers—Florida Area Cirrus Experiment. *Journal of Geophysical Research*, *112*, D08304. <https://doi.org/10.1029/2006JD007851>
- Ploeger, F., Günther, G., Konopka, P., Fueglistaler, S., Müller, M., Hoppe, C., et al. (2013). Horizontal water vapor transport in the lower stratosphere from subtropics to high latitudes during boreal summer. *Journal of Geophysical Research: Atmospheres*, *118*, 8111–8127. <https://doi.org/10.1002/jgrd.50636>
- Popp, P. J., Gao, R. S., Marcy, T. P., Fahey, D. W., Hudson, P. K., Thompson, T. L., et al. (2004). Nitric acid uptake on subtropical cirrus cloud particles. *Journal of Geophysical Research*, *109*, D06302. <https://doi.org/10.1029/2003JD004255>
- Popp, P. J., Marcy, T. P., Jensen, E. J., Kärcher, B., Fahey, D. W., Gao, R. S., et al. (2006). The observation of nitric acid-containing particles in the tropical lower stratosphere. *Atmospheric Chemistry and Physics*, *6*(3), 601–611. <https://doi.org/10.5194/acp-6-601-2006>
- Portmann, R. W., Solomon, S., Garcia, R. R., Thomason, L. W., Poole, L. R., & McCormick, M. P. (1996). Role of aerosol variations in anthropogenic ozone depletion in the polar regions. *Journal of Geophysical Research*, *101*(D17), 22,991–23,006. <https://doi.org/10.1029/96JD02608>
- Poulida, O., & Dickerson, R. R. (1996). Stratosphere-troposphere exchange in a midlatitude mesoscale convective complex. *Journal of Geophysical Research*, *101*(D3), 6823–6836. <https://doi.org/10.1029/95JD03523>
- Pundt, I., Pommerehne, J.-P., Chipperfield, M. P., Van Roozendaal, M., & Goutail, F. (2002). Climatology of the stratospheric BrO vertical distribution by balloon-borne UV-visible spectrometry. *Journal of Geophysical Research*, *107*(D24), 4806. <https://doi.org/10.1029/2002JD002230>
- Randel, W., Moyer, E., Park, M., Jensen, E., Bemath, P., Walker, K., & Boone, C. (2012). Global variations of HDO and HDO/H<sub>2</sub>O ratios in the upper troposphere and lower stratosphere derived from ACE-FTS satellite measurements. *Journal of Geophysical Research*, *117*, D06303. <https://doi.org/10.1029/2011JD016632>
- Ray, E. A., Rosenlof, K. H., Richard, E. C., Hudson, P. K., Cziczó, D. J., Loewenstein, M., et al. (2004). Evidence of the effect of summertime midlatitude convection on the subtropical lower stratosphere from CRYSTAL-FACE tracer measurements. *Journal of Geophysical Research*, *109*, D18304. <https://doi.org/10.1029/2004JD004655>
- Richter, J. H., Tilmes, S., Mills, M. J., Tribbia, J., Kravitz, B., MacMartin, D. G., et al. (2017). Stratospheric dynamical response and ozone feedbacks in the presence of SO<sub>2</sub> injections. *Journal of Geophysical Research: Atmospheres*, *122*, 12,557–12,573. <https://doi.org/10.1002/2017JD026912>
- Ridley, B. A., Walega, J. G., Dye, J. E., & Grahek, F. E. (1994). Distributions of NO, NO<sub>x</sub>, NO<sub>y</sub>, and O<sub>3</sub> to 12 km altitude during the summer monsoon season over New Mexico. *Journal of Geophysical Research*, *99*(D12), 25,519–25,534. <https://doi.org/10.1029/94JD02210>
- Saiz-Lopez, A., Baidar, S., Cuevas, C. A., Koenig, T. K., Fernandez, R. P., Dix, B., et al. (2015). Injection of iodine to the stratosphere. *Geophysical Research Letters*, *42*, 6852–6859. <https://doi.org/10.1002/2015GL064796>
- Salawitch, R. J., Weisenstein, D. K., Kovalenko, L. J., Sioris, C. E., Wennberg, P. O., Chance, K., et al. (2005). Sensitivity of ozone to bromine in the lower stratosphere. *Geophysical Research Letters*, *32*, L05811. <https://doi.org/10.1029/2004GL021504>
- Salawitch, R. J., Wofsy, S. C., Wennberg, P. O., Cohen, R. C., Anderson, J. G., Fahey, D. W., et al. (1994). The distribution of hydrogen, nitrogen, and chlorine radicals in the lower stratosphere: Implications for changes in O<sub>3</sub> due to the emission of NO<sub>y</sub> from supersonic aircraft. *Geophysical Research Letters*, *21*(23), 2547–2550. <https://doi.org/10.1029/94GL02781>
- Sander, S. P., Abbatt, J., Barker, J. R., Burkholder, J. B., Friedl, R. R., Golden, D. M., et al. (2011). Chemical kinetics and photochemical data for use in atmospheric studies, evaluation no. 17. Pasadena, CA: Jet Propulsion Laboratory
- Sang, W., Huang, Q., Tian, W., Wright, J. S., Zhang, J., Tian, H., et al. (2018). A large eddy model study on the effect of overshooting convection on lower stratospheric water vapor. *Journal of Geophysical Research: Atmospheres*, *123*(18), 10,023–10,036. <https://doi.org/10.1029/2017JD028069>
- Sargent, M. R., Smith, J. B., Sayres, D. S., & Anderson, J. G. (2014). The roles of deep convection and extratropical mixing in the tropical tropopause layer: An in situ measurement perspective. *Journal of Geophysical Research: Atmospheres*, *119*, 12,355–12,371. <https://doi.org/10.1002/2014JD022157>
- Sayres, D. S., Pfister, L., Hanisco, T. F., Moyer, E. J., Smith, J. B., Clair, M. S., et al. (2010). Influence of convection on the water isotopic composition of the tropical tropopause layer and tropical stratosphere. *Journal of Geophysical Research*, *115*, D00J20. <https://doi.org/10.1029/2009JD013100>
- Scheuer, E., Dibb, J. E., Twohy, C., Rogers, D. C., Heymsfield, A. J., & Bansemmer, A. (2010). Evidence of nitric acid uptake in the warm cirrus anvil clouds during the NASA TC4 campaign. *Journal of Geophysical Research*, *115*, D00J03. <https://doi.org/10.1029/2009JD012716>
- Schoeberl, M. R., & Dessler, A. E. (2011). Dehydration of the stratosphere. *Atmospheric Chemistry and Physics*, *11*(16), 8433–8446. <https://doi.org/10.5194/acp-11-8433-2011>
- Schoeberl, M. R., Dessler, A. E., & Wang, T. (2012). Simulation of stratospheric water vapor and trends using three reanalyses. *Atmospheric Chemistry and Physics*, *12*(14), 6475–6487. <https://doi.org/10.5194/acp-12-6475-2012>

- Schwartz, M. J., Read, W. G., Santee, M. L., Livesey, N. J., Froedeaux, L., Lambert, A., & Manney, G. L. (2013). Convectively injected water vapor in the North American summer lowermost stratosphere. *Geophysical Research Letters*, *40*, 2316–2321. <https://doi.org/10.1002/grl.50421>
- Scott, S. G., Bui, P. T., Chan, R. K., & Bowen, S. W. (1990). *Journal of Atmospheric and Oceanic Technology*, *7*(4), 525–540. [https://doi.org/10.1175/1520-0426\(1990\)007<0525:TMMSTO>2.0.CO;2](https://doi.org/10.1175/1520-0426(1990)007<0525:TMMSTO>2.0.CO;2)
- Shi, Q., Jayne, J. T., Kolb, C. E., & Worsnop, D. R. (2001). Kinetic model for reaction of ClONO<sub>2</sub> with H<sub>2</sub>O and HCl and HOCl with HCl in sulfuric acid solutions. *Journal of Geophysical Research*, *106*(D20), 24,259–24,274. <https://doi.org/10.1029/2000JD000181>
- Smith, J. B., Wilmouth, D. M., Bedka, K. M., Bowman, K. P., Homeyer, C. R., Dykema, J. A., et al. (2017). A case study of convectively sourced water vapor observed in the overworld stratosphere over the United States. *Journal of Geophysical Research: Atmospheres*, *122*, 9529–9554. <https://doi.org/10.1002/2017JD026831>
- Solomon, D. L., Bowman, K. P., & Homeyer, C. R. (2016). Tropopause-penetrating convection from three-dimensional gridded NEXRAD data. *Journal of Applied Meteorology*, *55*(2), 465–478. <https://doi.org/10.1175/JAMC-D-15-0190.1>
- Solomon, S. (1999). Stratospheric ozone depletion: A review of concepts and history. *Reviews of Geophysics*, *37*(3), 275–316. <https://doi.org/10.1029/1999RG900008>
- Solomon, S., Borrmann, S., Garcia, R. R., Portmann, R., Thomason, L., Poole, L. R., et al. (1997). Heterogeneous chlorine chemistry in the tropopause region. *Journal of Geophysical Research*, *102*(D17), 21,411–21,429. <https://doi.org/10.1029/97JD01525>
- Solomon, S., Garcia, R. R., Sherwood, F. S., & Wuebbles, D. J. (1986). On the depletion of Antarctic ozone. *Nature*, *321*(6072), 755–758. <https://doi.org/10.1038/321755a0>
- Solomon, S., Portmann, R. W., Garcia, R. R., Randel, W., Wu, F., Nagatani, R., et al. (1998). Ozone depletion at mid-latitudes: Coupling of volcanic aerosols and temperature variability to anthropogenic chlorine. *Geophysical Research Letters*, *25*(11), 1871–1874. <https://doi.org/10.1029/98GL01293>
- Solomon, S., Portmann, R. W., Garcia, R. R., Thomason, L. W., Poole, L. R., & McCormick, M. P. (1996). The role of aerosol variations in anthropogenic ozone depletion at northern midlatitudes. *Journal of Geophysical Research*, *101*(D3), 6713–6727. <https://doi.org/10.1029/95JD03353>
- Steinbrecht, W., Hegglin, M. I., Harris, N., & Weber, M. (2018). Is global ozone recovering? *Comptes Rendus Geoscience*, *350*(7), 368–375. <https://doi.org/10.1016/j.crte.2018.07.012>
- Stimpfle, R. M., Cohen, R. C., Bonne, G. P., Voss, P. B., Perkins, K. K., Koch, L. C., et al. (1999). The coupling of ClONO<sub>2</sub>, ClO, and NO<sub>2</sub> in the lower stratosphere from in situ observations using the NASA ER-2 aircraft. *Journal of Geophysical Research*, *104*(D21), 26,705–26,714. <https://doi.org/10.1029/1999JD900288>
- Stone, K. A., Solomon, S., & Kinnison, D. E. (2018). On the identification of ozone recovery. *Geophysical Research Letters*, *45*(10), 5158–5165. <https://doi.org/10.1029/2018GL077955>
- Sun, Y., & Huang, Y. (2015). An examination of convective moistening of the lower stratosphere using satellite data. *Earth and Space Science*, *2*, 320–330. <https://doi.org/10.1002/2015EA000115>
- Tabazadeh, A., Toon, O. B., Clegg, S. L., & Hamill, P. (1997). A new parameterization of H<sub>2</sub>SO<sub>4</sub>/H<sub>2</sub>O aerosol composition: Atmospheric implications. *Geophysical Research Letters*, *24*(15), 1931–1934. <https://doi.org/10.1029/97GL01879>
- Tegtmeier, S., Ziska, F., Pisso, I., Quack, B., Velders, G. J. M., Yang, X., & Krüger, K. (2015). Oceanic bromoform emissions weighted by their ozone depletion potential. *Atmospheric Chemistry and Physics*, *15*(23), 13,647–13,663. <https://doi.org/10.5194/acp-15-13647-2015>
- Thomason, L. W., Poole, L. R., & Deshler, T. (1997). A global climatology of stratospheric aerosol surface area density deduced from Stratospheric Aerosol and Gas Experiment II measurement: 1984–1994. *Journal of Geophysical Research*, *102*(D7), 8967–8976. <https://doi.org/10.1029/96JD02962>
- Thornton, B. F., Toohey, D. W., Tuck, A. F., Elkins, J. W., Kelly, K. K., Hovde, S. J., et al. (2007). Chlorine activation near the midlatitude tropopause. *Journal of Geophysical Research*, *112*(D18), D18306. <https://doi.org/10.1029/2006JD007640>
- Tilmes, S., Kinnison, D. E., Garcia, R. R., Salawitch, R., Canty, T., Lee-Taylor, J., et al. (2012). Impact of very short-lived halogens on stratospheric ozone abundance and UV radiation in a geo-engineered atmosphere. *Atmospheric Chemistry and Physics*, *12*(22), 10,945–10,955. <https://doi.org/10.5194/acp-12-10945-2012>
- Tilmes, S., Müller, R., & Salawitch, R. (2008). The sensitivity of polar ozone depletion to proposed geoengineering schemes. *Science*, *320*(5880), 1201–1204. <https://doi.org/10.1126/science.1153966>
- Toon, O. B., Maring, H., Dibb, J., Ferrare, R., Jacob, D. J., Jensen, E. J., et al. (2016). Planning, implementation, and scientific goals of the Studies of Emissions and Atmospheric Composition, Clouds, and Climate Coupling by Regional Surveys (SEAC<sup>4</sup>RS) field mission. *Journal of Geophysical Research: Atmospheres*, *121*, 4967–5009. <https://doi.org/10.1002/2015JD024297>
- Trapp, R. J., Dittenbaugh, N. S., & Gluhovsky, A. (2009). Transient response to severe thunderstorm forcing to elevated greenhouse gas concentrations. *Geophysical Research Letters*, *36*, L01703. <https://doi.org/10.1029/2008GL036203>
- Ullerstam, M., & Abbatt, J. P. D. (2005). Burial of gas-phase HNO<sub>3</sub> by growing ice surfaces under tropospheric conditions. *Physical Chemistry Chemical Physics*, *7*(20), 3596–3600. <https://doi.org/10.1039/b507797d>
- Vernier, J.-P., Pommereau, J.-P., Thomason, L. W., Pelon, J., Garnier, A., Deshler, T., et al. (2011). Overshooting of clean tropospheric air in the tropical lower stratosphere as seen by the CALIPSO lidar. *Atmospheric Chemistry and Physics*, *11*(18), 9683–9696. <https://doi.org/10.5194/acp-11-9683-2011>
- Voigt, C., Kärcher, B., Schlager, H., Schiller, C., Krämer, M., de Reus, M., et al. (2007). In-situ observations and modeling of small nitric acid-containing ice crystals. *Atmospheric Chemistry and Physics*, *7*(12), 3373–3383. <https://doi.org/10.5194/acp-7-3373-2007>
- Voigt, C., Schlager, H., Ziereis, H., Kärcher, B., Luo, B. P., Schiller, C., et al. (2006). Nitric acid in cirrus clouds. *Geophysical Research Letters*, *33*, L05803. <https://doi.org/10.1029/2005GL025159>
- von Hobe, M., Groß, J.-U., Günther, G., Konopka, P., Gensch, I., Krämer, M., et al. (2011). Evidence for heterogeneous chlorine activation in the tropical UTLS. *Atmospheric Chemistry and Physics*, *11*(1), 241–256. <https://doi.org/10.5194/acp-11-241-2011>
- Wales, P. A., Salawitch, R. J., Nicely, J. M., Anderson, D. C., Canty, T. P., Baidar, S., et al. (2018). Stratospheric injection of brominated very short-lived substances: Aircraft observations in the Western Pacific and representation in global models. *Journal of Geophysical Research: Atmospheres*, *123*(10), 5690–5719. <https://doi.org/10.1029/2017JD027978>
- Wang, P. K. (2003). Moisture plumes above thunderstorm anvils and their contributions to cross-tropopause transport of water vapor in midlatitudes. *Journal of Geophysical Research*, *108*(D6), D002581. <https://doi.org/10.1029/2002JD002581>
- Wang, P. K., Su, S.-H., Charvát, Z., Štáfka, J., & Lin, H.-M. (2011). Cross tropopause transport of water by mid-latitude deep convective storms: A review. *Terrestrial Atmospheric and Oceanic Studies*, *22*(5), 447–462. [https://doi.org/10.3319/TAO.2011.06.13.01\(A\)](https://doi.org/10.3319/TAO.2011.06.13.01(A))

- Weinstock, E. M., Pittman, J. V., Sayres, D. S., Smith, J. B., Anderson, J. G., Wofsy, S. C., et al. (2007). Quantifying the impact of the North American monsoon and deep midlatitude convection on the subtropical lowermost stratosphere using in situ measurements. *Journal of Geophysical Research*, *112*, D18310. <https://doi.org/10.1029/2007JD008554>
- Wennberg, P. O., Cohen, R. C., Stimpfle, R. M., Koplow, J. P., Anderson, J. G., Salawitch, R. J., et al. (1994). Removal of stratospheric O<sub>3</sub> by radicals: In situ measurements of OH, HO<sub>2</sub>, NO, NO<sub>2</sub>, ClO, and BrO. *Science*, *266*(5184), 398–404. <https://doi.org/10.1126/science.266.5184.398>
- Wilmouth, D. M., Stimpfle, R. M., Anderson, J. G., Elkins, J. W., Hurst, D. F., Salawitch, R. J., & Lait, L. R. (2006). Evolution of inorganic chlorine partitioning in the Arctic polar vortex. *Journal of Geophysical Research*, *111*, D16308. <https://doi.org/10.1029/2005JD006951>
- Wilson, J. C., Jonsson, H. H., Brock, C. A., Toohey, D. W., Avallone, L. M., Baumgardner, D., et al. (1993). In situ observations of aerosol and chlorine monoxide after the 1991 eruption of Mount Pinatubo: Effect of reactions on sulfate aerosol. *Science*, *261*(5125), 1140–1143. <https://doi.org/10.1126/science.261.5125.1140>
- World Meteorological Organization (2014). Scientific assessment of ozone depletion: 2014, Global Ozone Research and Monitoring Project-Report no. 55. Geneva, Switzerland: WMO.
- Yang, X., Abraham, N. L., Archibald, A. T., Braesicke, P., Keeble, J., Telford, P. J., et al. (2014). How sensitive is the recovery of stratospheric ozone to changes in concentrations of very short-lived bromocarbons? *Atmospheric Chemistry and Physics*, *14*(19), 10,431–10,438. <https://doi.org/10.5194/acp-14-10431-2014>
- Youn, D., Patten, K. O., Wuebbles, D. J., Lee, H., & So, C.-W. (2010). Potential impact of iodinated replacement compounds CF<sub>3</sub>I and CH<sub>3</sub>I on atmospheric ozone: A three-dimensional modeling study. *Atmospheric Chemistry and Physics*, *10*(20), 10,129–10,144. <https://doi.org/10.5194/acp-10-10129-2010>
- Ziska, F., Quack, B., Tegmeier, S., Stemmler, I., & Krüger, K. (2017). Future emissions of marine halogenated very-short lived substances under climate change. *Journal of Atmospheric Chemistry*, *74*(2), 245–260. <https://doi.org/10.1007/s10874-016-9355-3>
- Zondlo, M. A., Barone, S. B., & Tolbert, M. A. (1997). Uptake of HNO<sub>3</sub> on ice under upper tropospheric conditions. *Geophysical Research Letters*, *24*(11), 1391–1394. <https://doi.org/10.1029/97GL01287>